




## Anatomy and phylogenetic affinities of a new silesaurid assemblage from the Carnian beds of south Brazil

Gabriel Mestriner, Júlio C. A. Marsola, Sterling J. Nesbitt, Átila Augusto Stock Da-Rosa & Max Langer


To cite this article: Gabriel Mestriner, Júlio C. A. Marsola, Sterling J. Nesbitt, Átila Augusto Stock Da-Rosa & Max Langer (2023) Anatomy and phylogenetic affinities of a new silesaurid assemblage from the Carnian beds of south Brazil, *Journal of Vertebrate Paleontology*, 43:1, e2232426, DOI: [10.1080/02724634.2023.2232426](https://doi.org/10.1080/02724634.2023.2232426)


To link to this article: <https://doi.org/10.1080/02724634.2023.2232426>

 View supplementary material 

 Published online: 23 Aug 2023.

 Submit your article to this journal 

 Article views: 718

 View related articles 

 View Crossmark data 

 Citing articles: 5 View citing articles 

## ANATOMY AND PHYLOGENETIC AFFINITIES OF A NEW SILESAURID ASSEMBLAGE FROM THE CARNIAN BEDS OF SOUTH BRAZIL

GABRIEL MESTRINER, \*,<sup>1,2</sup> JÚLIO C. A. MARSOLA, <sup>1,3</sup> STERLING J. NESBITT, <sup>4</sup>  
ÁTILA AUGUSTO STOCK DA-ROSA, <sup>5</sup> and MAX LANGER <sup>1</sup>

<sup>1</sup>Departamento de Biologia, Universidade de São Paulo, Avenida Bandeirantes 3900, Ribeirão Preto 14040-190, Brazil, gabriel.mestriner93@gmail.com; juliomarsola@gmail.com; mclanger@ffclrp.usp.br;

<sup>2</sup>Department of Ecology and Evolutionary Biology, University of Toronto, 25 Willcocks Street, Toronto, ON M5S 3B2, Canada;

<sup>3</sup>Universidade Tecnológica Federal do Paraná, Campus Dois Vizinhos, 85660-000, Estrada para Boa Esperança, km 04, Paraná, Brazil;

<sup>4</sup>Department of Geosciences, Virginia Tech, Derring Hall 926 West Campus Drive, Blacksburg, VA 24061, U.S.A, sjn2104@vt.edu;

<sup>5</sup>Laboratório de Estratigrafia e Paleobiologia, Departamento de Geociências, Universidade Federal de Santa Maria, Santa Maria 97105-900, Rio Grande do Sul, Brazil, atiladarosa@gmail.com

**ABSTRACT**—New specimens and the reassessment of many silesaurids have recently shed light on the origin and early evolution of dinosaurs and their close relatives. Yet, the group is relatively poorly represented in South America, an area that likely played an important role in dinosaurian origins. Since the discovery of *Sacisaurus agudoensis* from the Norian Caturrita Formation, only the fragmentary *Gamatavus antiquus* and *Amanasaurus nesbitti* have been reported from the Triassic of south Brazil. Here we describe disarticulated silesaurid remains from Waldsanga, one of the most important tetrapod-bearing localities of the Santa Maria Formation, which represent the second Carnian occurrence of the group in Brazil. The postcranial elements exhibit a combination of dinosauromorph sympleiomorphies and silesaurid diagnostic traits, showing that a conservative anatomy is pervasive among early dinosauromorphs. We also conducted a set of exploratory analyses to infer the phylogenetic relations of the new occurrence and the robustness of some of the most recent phylogenetic hypotheses in face of the increasing diversity of Silesauridae. This revealed a rather uncertain evolutionary scenario not only for Silesauridae, but for early dinosauromorphs in general.

**SUPPLEMENTARY FILES**—Supplementary files are available for this article for free at [www.tandfonline.com/UJVP](http://www.tandfonline.com/UJVP).

Citation for this article: Mestriner, G., Marsola, J. C. A., Nesbitt, S. J., Da-Rosa, A. A. S., & Langer, M. (2023) Anatomy and phylogenetic affinities of a new silesaurid assemblage from the Carnian beds of south Brazil. *Journal of Vertebrate Paleontology*. <https://doi.org/10.1080/02724634.2023.2232426>

Submitted: December 9, 2022

Revisions received: June 16, 2023

Accepted: June 28, 2023

First published online: August 23, 2023

### INTRODUCTION

The evolutionary radiation of dinosaurs in the Late Triassic was a milestone event in the history of the Earth (Brusatte et al., 2008, 2010; Benton et al., 2014; Langer et al., 2010, 2013). The group was exceptionally successful in terrestrial ecosystems during the Mesozoic Era, and one subgroup, birds, remain as an important component of modern ecosystems (Brusatte et al., 2010). Dinosaurs are part of the larger clade Dinosauromorphia, which includes a variety of non-dinosaurian lineages temporally restricted to the Middle–Late Triassic (Brusatte et al., 2010; Langer, 2014). In this context, silesaurids play an important role for understanding the origin and evolution of Dinosauria and the key features that promoted their early

radiation and evolutionary success (Benton et al., 2014; Brusatte et al., 2008, 2010; Langer et al., 2010, 2013; Marsola et al. 2019b; Mestriner et al., 2022).

Silesauridae is a group of gracile dinosauriforms of 1–3 meters in length, with long hindlimbs and slender arms, known from the Middle Triassic to the Norian of South and North America, Africa, and Europe (Benton et al., 2014; Dzik, 2003; Irmis et al., 2007; Langer et al., 2010, 2013; Nesbitt et al., 2010). According to the most recent reviews, the group includes *Lewisuchus admixtus* Romer, 1972, *Eucoelophys baldwini* Sullivan & Lucas, 1999, *Silesaurus opolensis* Dzik, 2003, *Sacisaurus agudoensis* Ferigolo & Langer, 2007, *Asilisaurus kongwe* Nesbitt et al., 2010, *Diodorus scytobrachion* Kammerer et al., 2011, *Ignotosaurus fragilis* Martínez et al., 2012, *Lutungutali sitwensis* Peacock et al., 2013, *Kwanasaurus williamparkeri* Martz & Small, 2019, *Gamatavus antiquus* Pretto et al., 2022, and *Amanasaurus nesbitti* Müller & Garcia, 2023. Controversial silesaurid records include *Pisanosaurus mertii* Casamiquela, 1967, *Technosaurus smalli* Chatterjee, 1984, and *Soumyasaurus aenigmaticus* Sarigul et al., 2018 (see Agnolín & Rozadilla, 2018; Irmis et al., 2007; Sarigul et al., 2018).

\*Corresponding author.

This article was originally published with errors, which have now been corrected in the online version. Please see Correction (<http://dx.doi.org/10.1080/02724634.2023.2254075>)

Color versions of one or more of the figures in the article can be found online at [www.tandfonline.com/ujvp](http://www.tandfonline.com/ujvp).

Silesaurids have controversial phylogenetic relations among Dinosauriformes; in most hypotheses they are recovered as the sister-group of Dinosauria (Baron et al., 2017a; Benton & Walker 2011; Bittencourt et al., 2015; Langer et al., 2010, 2017; Nesbitt, 2011; Nesbitt et al., 2017a), whereas others suggest its nesting within the ornithischian lineage (Cabreira et al., 2016; Ferigolo & Langer, 2007; Langer & Ferigolo, 2013). Recently, Müller and Garcia (2020) and Norman et al. (2022) proposed Silesauridae as a paraphyletic group leading to core-ornithischians. Besides their phylogenetic importance, silesaurids are paleoecologically intriguing because they represent the earliest pan-avians with cranial and dental specializations for an omnivorous and/or herbivorous diet (Cabreira et al., 2016; Langer & Ferigolo, 2013; Nesbitt et al., 2010; Qvarnström et al., 2019).

In the context of the origins and evolution of early dinosaurs, South America plays a key role as the cradle of the first members of the lineage (Langer et al., 2017; Marsola et al., 2019b; Novas et al., 2021). Since the discovery of *Sacisaurus agudoensis* from the Norian Caturrita Formation of south Brazil (Ferigolo & Langer, 2007; Marsola et al., 2018), only two other silesaurids were reported in the country—the unambiguous Middle Triassic *Gamatavus antiquus* (Pretto et al., 2022) and the Carnian *Amanasaurus nesbitti* (Müller & Garcia, 2023). Here, we describe disarticulated silesaurid remains from the Waldsanga locality (Langer, 2005a, b), one of the most fruitful tetrapod-bearing sites of the Santa Maria Formation. This represents the second Carnian occurrence of the group in Brazil and the only based on more abundant skeletal remains. We also conduct a set of exploratory phylogenetic analyses to investigate the affinities of those remains and the robustness of some of the most recent phylogenetic hypotheses for dinosauromorphs in the face of the increasing diversity of Silesauridae.

## GEOLOGICAL SETTING

The specimens described here were unearthed from deposits of the Alemoa Member of the Santa Maria Formation, at the locality known as Waldsanga (Fig. 1; Huene, 1942; Langer, 2005b; Langer et al., 2007) or Cerro da Alemoa (Da Rosa, 2004, 2015). This site also yielded the type-specimens of the early sauropodomorph *Saturnalia tupiniquim* (Langer et al., 1999), the cynodonts *Gomphodontosuchus brasiliensis* (Huene, 1928; Langer, 2005a) and *Alemoatherium huebneri* (Martinelli et al., 2017), and the possible theropod dinosaur *Nhandumirim waldsangae* (Marsola et al., 2019a). Yet, the most abundant fossils from this locality are referred to the rhynchosaur *Hyperodapedon* (Langer et al., 2007).

The main lithology of the site is composed of massive, reddish mudstones of the Alemoa Member, overlaid by the yellowish to orange stratified sandstones of the Caturrita Formation (Fig. 1E; Marsola et al., 2019a, 2019b). The lower and intermediate levels of the Alemoa Member in the site represent distal floodplain deposits, whereas the upper level represents more proximal settings (Da Rosa 2005, 2015; Marsola et al., 2019a). According to previous stratigraphy studies (Horn et al., 2014), the strata exposed at Waldsanga belong to the Candelária Sequence, Santa Maria Supersequence (Santa Maria 2 Sequence of Zerbass et al., 2003), including the upper part of the Santa Maria Formation (Gordon, 1947) and the lower part of the Caturrita Formation (Andreis et al., 1980). In addition, the occurrence of *Hyperodapedon* rhynchosaurs justifies correlating the Alemoa member in the site to the *Hyperodapedon* AZ (Schultz et al., 2020). Correlations with radioisotopically dated strata from the Ischigualasto Formation (Ischigualasto–Villa Unión Basin) in western Argentina (e.g., Desojo et al., 2020; Martínez et al., 2011, 2012) that share a similar faunal association (e.g., Langer, 2005b; Langer et al., 2007) indicate that the *Hyperodapedon* AZ is late Carnian in age. This was corroborated by

detrital zircon radiometric dating in the Waldsanga site, which yielded a maximum age of ca. 233 Ma (Langer et al., 2018).

**Institutional Abbreviations**—**CRILAR-Pv**, Centro Regional de Investigaciones Científicas y Transferencia Tecnológica, Anillaco, Argentina; **FFCLRP**, Faculdade de Filosofia, Ciências e Letras de Ribeirão Preto, Ribeirão Preto, Brazil; **MCN**, Museu de Ciências Naturais, Fundação Zoobotânica do Rio Grande do Sul, Porto Alegre, Brazil; **MCP**, Museu de Ciências e Tecnologia da Pontifícia Universidade Católica do Rio Grande do Sul, Porto Alegre, Brazil; **MCZ**, Museum of Comparative Zoology, Harvard University, Cambridge, MA, U.S.A.; **NHMUK PV**, Natural History Museum, London, Palaeontology Vertebrates, London, U.K.; **NMT**, National Museum of Tanzania, Dar es Salaam, Tanzania; **PVSJ**, División de Paleontología de Vertebrados del Museo de Ciencias Naturales y Universidad Nacional de San Juan, San Juan, Argentina; **SAM**, Iziko South African Museum, Cape Town, South Africa; **UFSM**, Universidade Federal de Santa Maria, Santa Maria, Brazil; **ZPAL**, Institute of Paleobiology of the Polish Academy of Sciences, Warsaw, Poland.

## MATERIAL AND METHODS

### Phylogenetic Analyses

UFSM 11579 was first included in the data matrix of Baron et al. (2017a), as modified by Langer et al. (2017), Nesbitt et al. (2019), and finally Ezcurra et al. (2019). We chose this data matrix because of its inclusiveness and more comprehensive data on taxa such as *Asilisaurus kongwe* and *Lewisuchus admixtus*. Following Agnolin & Ezcurra (2019) the taxon name *Marasuchus* was updated to *Lagosuchus talampayensis*. We were able to reproduce Ezcurra et al. (2019) results only when the old scores for *Lewisuchus admixtus* (*LewisuchusPseudolagosuchus* in their matrix) and *Asilisaurus kongwe* (*Asilisaurus* in their matrix) were excluded from the analysis. Hence, we considered only the new scores (*Asilisaurus\_new\_scores* and *Lewisuchus\_new\_scores* in their matrix). Even though Ezcurra et al. (2019) mentioned that they updated the scorings of those two taxa and explored its implications for the phylogenetic analysis, they do not explicitly state whether the old scores were excluded or not. However, as we were only able to reproduce their topology by excluding the old scores of both taxa, we assumed that Ezcurra et al. (2019) considered only the new scores, although not excluding the old ones from the NEXUS file found in the ‘supporting information’ document. Also, it is important to mention that a warning message appears when the file is read in TNT, communicating that character 303 for taxon 38 and character 333 for taxon 52 were converted to range. We understand that this might be related to the fact that both characters are ordered and coded as “0&2,” which the program might interpret as an indication that they have three character states. We did not explore this further because it goes beyond the scope of this work. Moreover, we added *Nhandumirim waldsangae* to increase the early dinosaur sampling of this dataset. We also modified the scores of character 161 (corresponding to the tooth attachment mode) from “1” to “0&1,” for *Asilisaurus kongwe*, *Sacisaurus agudoensis*, and *Eucoelophysis baldwini*, given its plasticity as shown by Mestriner et al. (2022). The final matrix (counting the pruned taxa) has 85 taxa and 457 characters, in which characters 24, 35, 39, 60, 68, 71, 117, 145, 167, 169, 174, 180, 197, 199, 206, 214, 215, 222, 251, 269, 272, 286, 289, 303, 305, 307, 313, 322, 333, 334, 338, 353, 360, 376, 378, 387, 393, 442, and 446 were ordered. The data matrix was analyzed under equally weighted parsimony using TNT v.1.5 (Goloboff et al., 2008; Goloboff & Catalano, 2016), with *Euparkeria capensis* (Archosauriformes non-Archosauria) designated as the operational outgroup. Following Ezcurra et al. (2019) we did a new technology search with 100 hits (“find min. length, 100”) and changed the “Init. Addseqs”

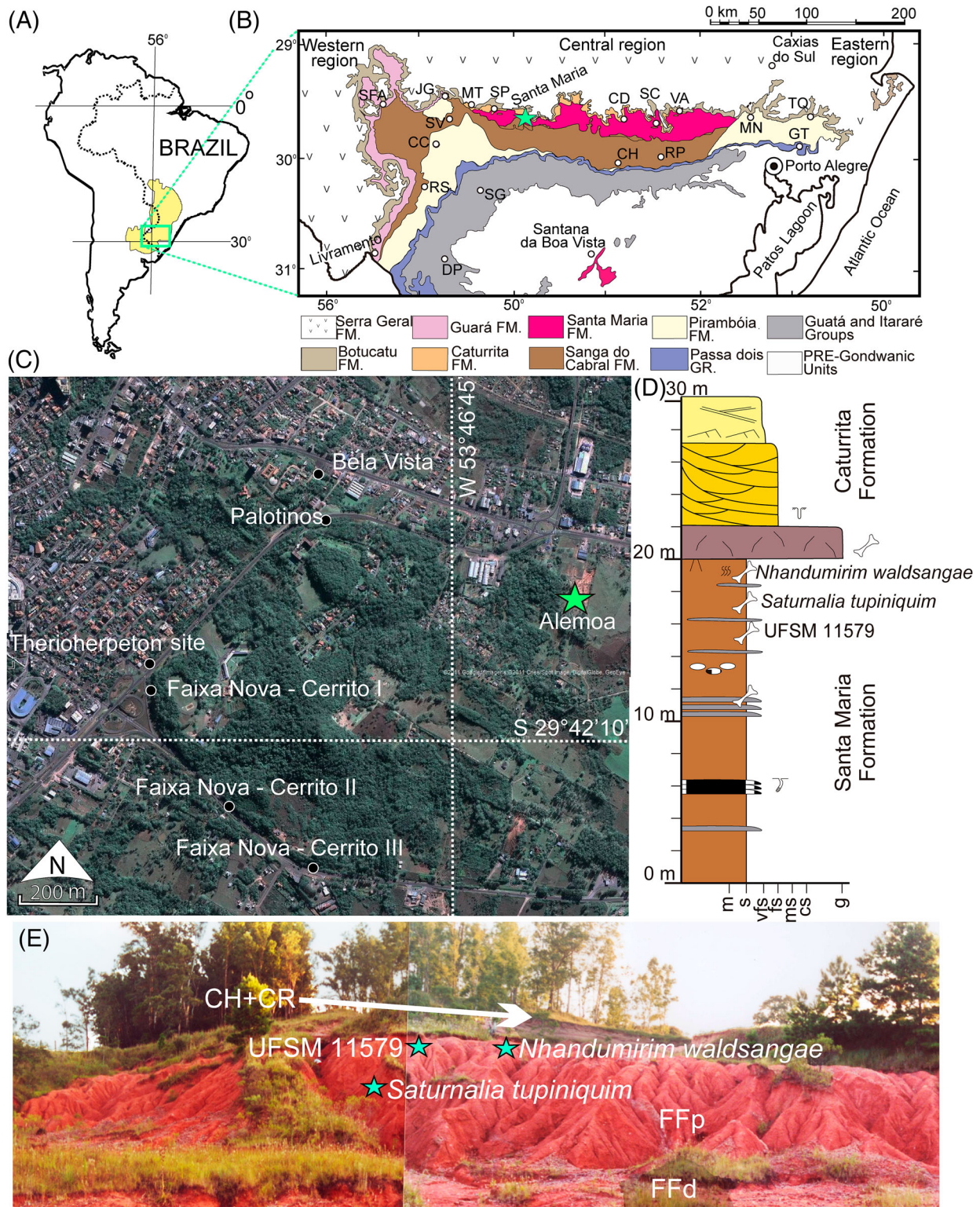


FIGURE 1. Geographic and geological provenance of UFSM 11579. **A**, map of the Paraná Basin in South America; **B**, simplified geological map of the central portion of Rio Grande do Sul State (modified from Eltink et al., 2017), indicating Santa Maria; **C**, location of selected outcrops in the eastern outskirts of Santa Maria (modified from Da Rosa, 2015), indicating the Waldsanga/Cerro da Alemoa site; **D**, sedimentary log from the Waldsanga/Cerro da Alemoa outcrop, indicating the provenance of the studied specimen and other fossiliferous beds (modified from Da Rosa, 2005); **E**, photograph of the outcrop, showing the channel and crevasse deposits (CH + CR) of the Caturrita Formation and the distal (FFd) and proximal (FFp) floodplain deposits of the Santa Maria Formation, specifying the level where UFSM 11579 was found, which was near from where the early theropod *Nhandumirim waldsangae* and the early sauropod *Saturnalia tupiniquim* were discovered. Modified from Marsola et al. (2019a). **Abbreviations:** CC, Cacequi; CD, Candelária; CH, Cachoeira do Sul; CH + CR, channel and crevasse deposits; cs, coarse sand; DP, Dom Pedrito; FFd, distal floodplain deposit; FFp, proximal floodplain deposit; FM, Formation; fs, fine sand; g, gravel; GR, Group; GT, Gravataí; JG, Jaguarí; m, mud; MN, Montenegro; ms, medium sand; MT, Mata; RP, Rio Pardo; RS, Rosário do Sul; s, silt; SC, Santa Cruz do Sul; SFA, São Francisco de Assis; SG, São Gabriel; SP, São Pedro do Sul; SV, São Vicente do Sul; TQ, Taquara; VA, Venâncio Aires; vfs, very fine sand.

default from 5 to 10. Lastly, we marked the option “collapse trees after the search”. The rest was kept as default. Branch support was calculated using decay indices (Bremer support values) and a bootstrap resampling analysis (using 1000 pseudoreplicates and reporting both absolute and GC frequencies, which corresponds to “Group present/Contradicted” and produces meaningful evaluations of the support for all groups, not only for those with absolute frequency above 0.5; Goloboff et al., 2003). Given the scope of this paper, the results of this first analysis are seen only in the [Supplemental Data](#). We equally followed Ezcurra et al. (2019) by rerunning the analysis with the a posteriori pruning of *Lutungutali sitwensis*, and also performed a third analysis with the same parameters, *Lutungutali sitwensis* still pruned, but excluding character 161. The results of these two latter analyses are discussed at the end of this document.

Subsequently, UFSM 11579 was included the dataset of Müller and Garcia (2020). In our analysis of the Müller and Garcia (2020) dataset we modified the scores of character 100—which corresponds to character 161 of Ezcurra et al. (2019)—as indicated above. The final matrix has 63 taxa and 277 characters, in which characters 4, 13, 18, 25, 63, 82, 84, 87, 89, 109, 142, 166, 174, 175, 184, 186, 190, 201, 203, 205, 209, 212, 225, 235, 236, 239, 250, and 256 were ordered. *Euparkeria capensis* (Archosauriformes non-Archosauria) was also designated as the operational outgroup. The data were analyzed under maximum parsimony in TNT 1.5 (Goloboff et al., 2008; Goloboff & Catalano, 2016), and only the “traditional search” was used. The heuristic search was performed under the following parameters: 10,000 replications of Wagner Trees (with random addition sequence); TBR (tree bisection and reconnection) for branch swapping; hold = 20 (trees saved per replicate); and collapse of zero-length branches according to ‘rule 1’ in TNT (Coddington & Scharff, 1994; Goloboff et al., 2008). The resulting most parsimonious trees (MPTs) were subject to a second round of TBR to ensure that all MPTs were found. Branch support (Bremer support values) and bootstrap values were calculated as for Ezcurra et al. (2019). We also performed a second analysis with the same parameters mentioned above, but excluding character 100. The results of the two analyses of the Müller and Garcia (2020) dataset are discussed at the end of this document. The NEXUS files of both Ezcurra et al. (2019) and Müller and Garcia (2020) data matrices used in our study are available in the Supplementary Material, Appendices S1 and S2, respectively.

### CT Scanning

Image stacks of the UFSM 11579 left maxilla (see Fig. 5) were acquired using a SkyScan 1172 located at Virginia Tech with the following parameters: 70 kV voltage, 142  $\mu$ A current, and 10 W power. The scanning of all the other materials were acquired at “Centro para Documentação da Biodiversidade,” Universidade de São Paulo at Ribeirão Preto, using the micro-CT scanning GE Phoenix|tomex S240, with 1000 projections, exposure time of 0.3 s, voltage of 130 Kv, and a current of 150  $\mu$ A, with a voxel size of 25.8  $\mu$ m. We used “Avizo” (v. 7.0.0) to virtually and manually segment the cranial bones. The raw CT scan data are available in the following repository: <https://doi.org/10.5281/zenodo.7939011>.

### Femoral Histology

The shaft of one left femur (UFSM 11579O) was transversely sectioned right below the fourth trochanter so that one thin-slice was produced to examine its histology. The material was fully embedded in Castolite AC polyester resin in a plastic container and then peroxide catalyst was incorporated in a ratio of 10 methyl ethyl ketone peroxide drops for 30 ml of resin. Then, the material was vacuumed for 5 min to evacuate all air bubbles. After cutting, the surfaces were polished using 600

and 1000 grit silicon carbide powder. The samples were left to dry for 24 hours and mounted to plexiglass frosted slides. Once fixed, the thick sections were cut using the *Isomet 1000* at a trim thickness of approximately 0.7 mm. The specimens were then ground down using a grinding machine. The sections were constantly checked under the microscope until they nearly reached the desired optical clarity. Once the slide was reaching the desired thickness, the final grinding was done by hand with 1-micron aluminum oxide powder.

## SYSTEMATIC PALEONTOLOGY

DINOSAURIFORMES Novas, 1992, sensu Ezcurra, Nesbitt, Fiorelli, & Desojo, 2019

SILESAURIDAE Langer, Ezcurra, Bittencourt, & Novas, 2010

UFSM 11579A-V (Figs. 2–15) is an assemblage of disarticulated cranial and postcranial elements comprising multiple individuals (Fig. 2), including one right and two left maxillae, three lower jaw fragments, one cervical vertebra, one incomplete cervical rib, one right scapula, two right ilia, three left and three right femora, two left tibiae, two right fibulae, and one non-ungual phalanx of uncertain position.

The bones were found in close association and have matching taphonomic signatures. As the specimens share a similar phylogenetic signal and duplicated elements have a close morphology (when present, variations are mentioned accordingly) they are tentatively described as part of a single taxonomic unit. The material is housed at Laboratório de Estratigrafia e Paleobiologia, Universidade Federal de Santa Maria, Brazil. All the measurements were made manually using a caliper (listed in Table 1).

## RESULTS

### Osteological Description

**Maxilla**—There are three incomplete maxillae (two left and one right), each preserving different parts (Figs. 3–6). The alveoli numbers serve here only for descriptive purposes and do not reflect their original positions in the bones. The better-preserved element (UFSM 11579A) is from the left side, preserving the antorbital fenestra and five tooth positions (Figs. 3, 4A). One of the right maxillae (Fig. 5; UFSM 11579B) lacks most of the antorbital fenestra, preserving only its ventral margin. This is represented by an anteroposteriorly elongated piece of bone containing eight tooth positions (Fig. 5C). The third maxilla is a small fragment from the left side (UFSM 11579C), which has four tooth positions preserved, with two broken tooth fragments at the first and third alveoli (Fig. 6A). This specimen was mentioned in a previous survey (Mestriner et al., 2022).

The only fully erupted tooth of UFSM 11579A is at the second preserved position (Fig. 3), just ventral to the anterior margin of the external antorbital fenestra. It is firmly implanted in the alveolus, leaving no apparent space around the dentine. The four empty alveoli are better identified in the 3D model reconstruction (Fig. 3). The third alveolus has a rounded socket in ventral view. The first alveolus is located at the anterior-most preserved portion, and only its posterior edge is preserved (Fig. 3E). The sockets of the fourth and fifth alveoli are not well preserved, but outlines and shallow excavations indicate their positions. UFSM 11579B shows eight tooth positions, preserving erupted teeth at the first, third, fifth, sixth, and eighth alveoli. Its anterior end is dorsoventrally flattened (Fig. 5C).

As only preserved in the flat lateral surface of UFSM 11579A, there are two foramina immediately ventral to the antorbital fossa and a distinct depression excavating the bone anteriorly to that fossa. The ventral edge of this depression is marked by

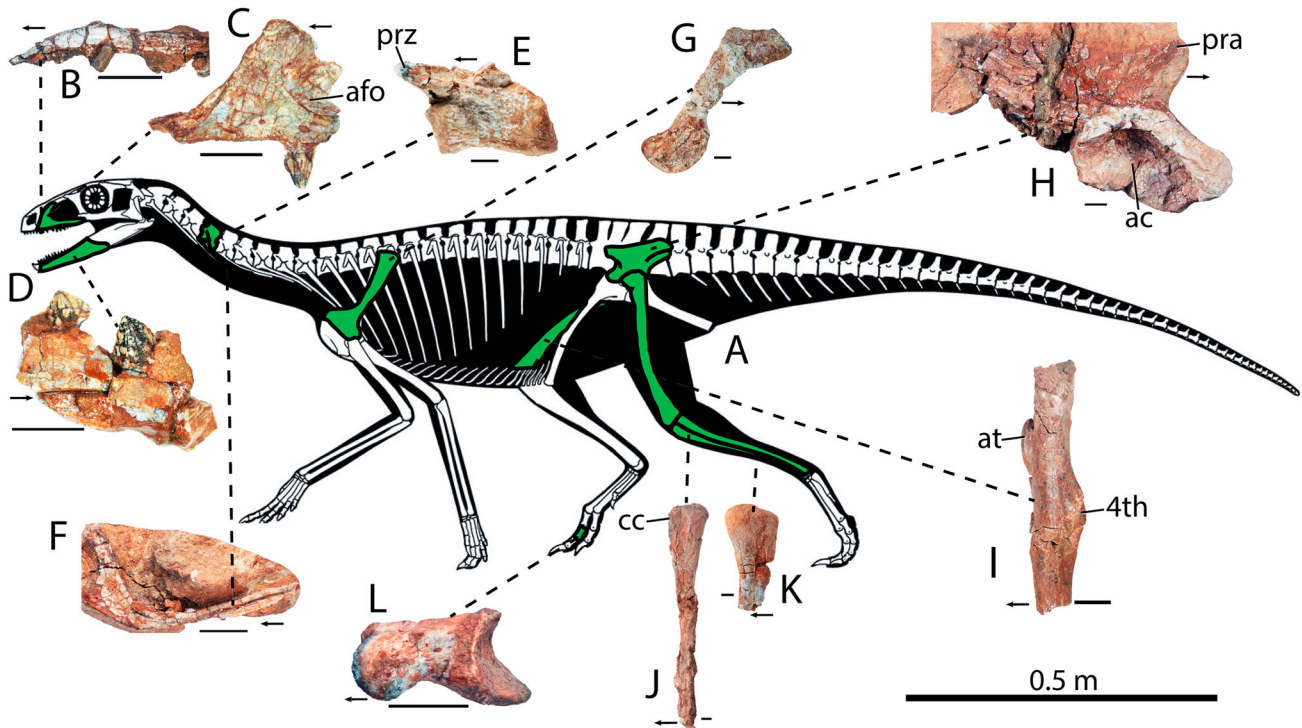


FIGURE 2. **A**, silhouette depicting the preserved bones of UFSM 11579, individual bones referred to UFSM 11579; **B**, right maxilla piece (UFSM 11579B) in medial view; **C**, left maxilla in lateral view (UFSM 11579A); **D**, right lower jaw piece in lateral view (UFSM 11579E); **E**, cervical vertebra (UFSM 11579G) in lateral view; **F**, cervical rib piece in lateral view (UFSM 11579H); **G**, right scapula (UFSM 11579I) in lateral view; **H**, right ilium (UFSM 11579J) in lateral view; **I**, right femur (UFSM 11579M) in anterior view; **J**, left tibia (UFSM 11579S) in lateral view; **K**, left fibula (UFSM 11579 T) in lateral view; **L**, indeterminate non-ungual pedal phalanx (UFSM 11579 V) in lateral/medial? view. Reconstruction of skeleton completed by Scott Hartman and figure extracted and modified from Nesbitt et al. (2019). Scale bars from **B** to **L** equal 0.5 cm. **Abbreviations:** ac, acetabulum; afo, antorbital fossa; at, anterior trochanter; cc, cnemial crest; pra, preacetabular ala; prz, prezygapophysis.

a ridge (Fig. 3A1–A3, B1, B2). This ridge extends subparallel to the alveolar margin, but strongly curves ventrally anterior to the first foramen (Fig. 3B1, B2), as seen in *Lewisuchus admixtus* (Ezcurra et al., 2019), but not in other silesaurids (e.g., *Asilisaurus kongwe*: NMT RB159; *Silesaurus opolenis*: ZPAL Ab III/361/26; *Sacisaurus agudoensis*: MCN PV10050—Ezcurra et al., 2019) and *Teleocrater rhadinus* (Nesbitt et al., 2017b). The boundary between the lateral surface of the maxilla and the antorbital fossa has an expanded ridge defining the margin of the external antorbital fenestra. Only its anterior end is preserved, dorsal to and posterior to the second foramen. A similar ridge was reported for *Eoraptor lunensis* (PVSJ 512) and *Coelophysis bauri* (MCZ 4326, 4327), but is unseen in most archosauriforms (e.g., *Euparkeria capensis*, SAM PK- K6047), including *Teleocrater rhadinus* (Nesbitt et al., 2017b).

The antorbital fossa excavates both the posterior and the dorsal rami of the maxilla. In the latter, the margin of the external antorbital fenestra is subtle (Figs. 3A, 4A), differing from the more abrupt edge seen in *Sacisaurus agudoensis* and *Silesaurus opolenis* (Dzik, 2003; Ferigolo & Langer, 2007; Langer & Ferigolo, 2013; Fig. 4B, C). In its anterior portion, the ventral margin of the external antorbital fenestra is subparallel to that of the maxilla, as typical of other silesaurids (e.g., *Sacisaurus agudoensis*; Fig. 4B).

The anterior portion of the antorbital fossa is lateromedially deeper (Figs. 3F, 4A) than that of *Sacisaurus agudoensis* (Fig. 4B) and *Silesaurus opolenis* (Fig. 4C), but similar to that of *Teleocrater rhadinus* (Nesbitt et al., 2017a, 2017b). The antorbital fossa wall is formed by a lateromedially flattened sheet of bone, which seems to extend more posteriorly than those of other silesaurids such as *Sacisaurus agudoensis* and *Silesaurus*

*opolenis* (Fig. 4). The anterior margin of the antorbital fossa is perforated as in various dinosaurs (Fig. 3F—Butler et al., 2008; Langer & Ferigolo, 2013; Martinez et al., 2011; Rauhut, 2003; Tykoski, 2005; Witmer, 1997), diverging from the condition in most silesaurids (Fig. 4B, C—Langer & Ferigolo, 2013). The anterodorsal margin of the maxilla is slightly concave (Fig. 3A), whereas the lateral margin of its anteromedial process is concave and anteroposteriorly outlined by a diagonal crest ('pmac' in Fig. 3A), likely for the articulation of the premaxilla.

On the medial surface, a well-developed palatal process forms a protruding shelf that parallels the alveolar margin. It has a well-defined ventral surface and is dorsoventrally thicker anteriorly, near the preserved tooth (Fig. 3C). Interdental plates are seen surrounding the teeth medially (Fig. 3C2, C3, D2), as is typical of crocodiles, silesaurids, and dinosaurs (LeBlanc et al., 2017; Mestriner et al., 2022).

**Dentary**—Three lower jaw fragments were recovered (UFSM 11579D–F; Fig. 6B–D). The dentary slightly tapers toward the anterior portion, with an evident Meckelian canal seen in medial view paralleling the ventral margin of the bone (Fig. 6B2). Two ovoid foramina are seen in the lateral surface of the bone, near the first and third tooth positions as preserved (Fig. 6B1). Interdental plates are present laterally, medially, and between the teeth (Fig. 6B2, B3). Medially, there is an edge delimiting the interdental plate/jaw bone contact (Fig. 6B2). A conspicuous ridge extends along the lateral/medial? surface of the dentary, right at the contact between the interdental plate and the jaw bone ('r' in Fig. 6D1).

**Dentition**—All preserved teeth are firmly embedded in the alveoli, leaving no space around the dentine (Figs. 3, 5, 6). The

TABLE 1. Postcranial measurements (Note: values are given in centimeters).

Measurement info:	Specimen:		
Cervical Vertebra:	UFSM 11579G:		
Centrum anteroposterior length	2.2		
Centrum maximum dorsoventral length	0.9		
Centrum lateromedial width	1.2		
Prezygapophysis length	1.2		
Scapula:	UFSM 11579I:		
Maximum anteroposterior length	5.5		
Maximum lateromedial width	1.5		
Maximum width of the blade axis	1.0		
Minimal anteroposterior width of the blade axis	0.7		
Ilia:	UFSM 11579J:	UFSM 11579K:	
Maximum anteroposterior length	7.0	NA	
Maximum dorsoventral height	3.5	NA	
Iliac blade maximum length	5.5	NA	
Iliac blade maximum height	1.5	NA	
Acetabulum width	1.5	1.5	
Acetabulum dorsoventral height	2.1	NA	
Acetabulum anteroposterior length	2.7	2.6	
Length of the pubic peduncle	2.2	NA	
Brevis fossa width	NA	0.9	
Right Femora:	UFSM 11579L:	UFSM 11579M:	UFSM 11579N:
Dorsoventral length	11.2	NA	NA
Maximum width of the head (lateromedially)	1.9	1.8	1.8
Anteroposterior length of the head	1.0	0.7	0.7
Mediolateral width of the distal end	2.5	NA	NA
Anteroposterior length of the distal end	1.6	NA	NA
Popliteal fossa proximodistal extension	4.4	NA	NA
4th trochanter proximodistal length	1.1	1.7	NA
4th trochanter lateromedial width	0.5	0.5	NA
Anterior trochanter proximodistal length	1.0	1.2	1.2
Anterior trochanter lateromedial width	0.4	0.4	0.4
Dorsolateral trochanter proximodistal length	1.3	1.1	NA
Dorsolateral trochanter lateromedial width	0.4	0.3	NA
Left Femora:	UFSM 11579O:	UFSM 11579P:	UFSM 11579Q:
Dorsoventral length	10	NA	NA
Maximum width of the head (lateromedially)	1.7	2.3	NA
Anteroposterior length of the head	0.6	1.2	NA
Mediolateral width of the distal end	NA	NA	2.7
Anteroposterior length of the distal end	NA	NA	2.0
Popliteal fossa proximodistal extension	4.2	NA	3.9
4th trochanter proximodistal length	NA	NA	NA
4th trochanter lateromedial width	NA	NA	NA
Anterior trochanter proximodistal length	1.2	1.6	NA
Anterior trochanter lateromedial width	0.4	0.6	NA
Dorsolateral trochanter proximodistal length	NA	0.9	NA
Dorsolateral trochanter lateromedial width	NA	0.4	NA
Tibiae:	UFSM 11579R:	UFSM 11579S:	
Proximal end maximum lateromedial width	1.8	1.2	
Anteroposterior length of the proximal end	2.8	1.8	
Proximodistal length of the cnemial crest	1.6	1.6	
Anteroposterior length of the cnemial crest	0.7	0.6	
Fibula:	UFSM 11579T:	UFSM 11579U:	
Proximal end maximum lateromedial width	0.8	0.5	
Anteroposterior length of the proximal end	1.7	1.5	
Phalanx:	UFSM 11579V:		
Maximum anteroposterior length	2.2		
Minimum anteroposterior length	1.8		
Maximum lateromedial length	1.6		
Minimum lateromedial length	1.1		

tooth emerging from the left maxilla (UFSM 11579A) has the typical Silesauridae sub-triangular and leaf-shaped morphology in labial/lingual views (Fig. 3B1, B2, C3, D). Its crown base is

mesio-distally expanded and bears labial and lingual cinguli (Fig. 3B1, B2, C3, D, E). These are continuous to longitudinal prominent ridges that extend apicobasally along the center of

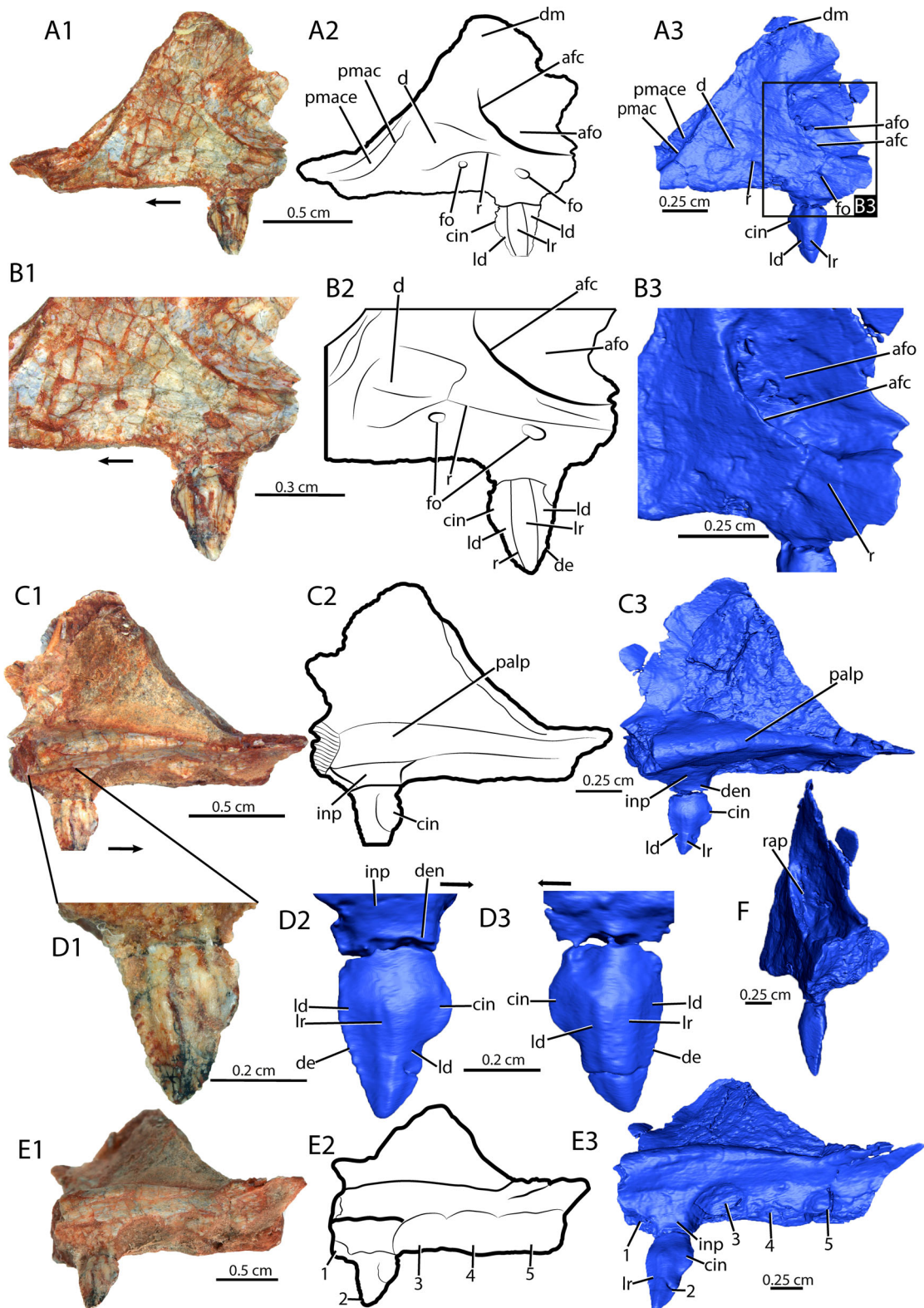


FIGURE 3. UFSM 11579A, left maxilla: **A1**, lateral view. **A2**, drawing highlighting the structures of A1; **A3**, UFSM 11579A digitally reconstructed by CT-scan segmentation, lateral view; **B1**, lateral view proximate and focusing on details of the preserved tooth and the ventral portion of the antorbital fenestra; **B2**, drawing highlighting the structures of B1; **B3**, the digital image of the CT-scan segmentation focusing on details of the ventral portion of the antorbital fenestra; **C1**, medial view; **C2**, drawing highlighting the structures of C1; **C3**, medial view of the UFSM 11579A digitally reconstructed by CT-scan segmentation; **D1**, proximate image of the tooth in medial view; **D2**, tooth digitally reconstructed by CT-scan segmentation, medial view; **D3**, tooth digitally reconstructed by CT-scan segmentation, lateral view; **E1**, dorsomedial view; **E2**, drawing highlighting the structures of E1; **E3**, UFSM 11579A digitally reconstructed by CT-scan segmentation, dorsomedial view; **F**, posterolateral view showing the wide antorbital fossa and the rostral aperture. **Abbreviations:** afo, antorbital fossa; afc, crest of antorbital fenestra; cin, cingulum; d, depression; de, denticles; den, dentine; dm, dorsal margin; fo, foramen; inp, interdental plate; ld, longitudinal depression; lr, longitudinal ridge; palp, palatal process. pmac, premaxilla contact; pmace, premaxilla contact excavation; r, ridge; rap, rostral aperture. Numbers indicate the alveoli position, from the anterior to the posterior portion. Arrows indicate the anterior direction.



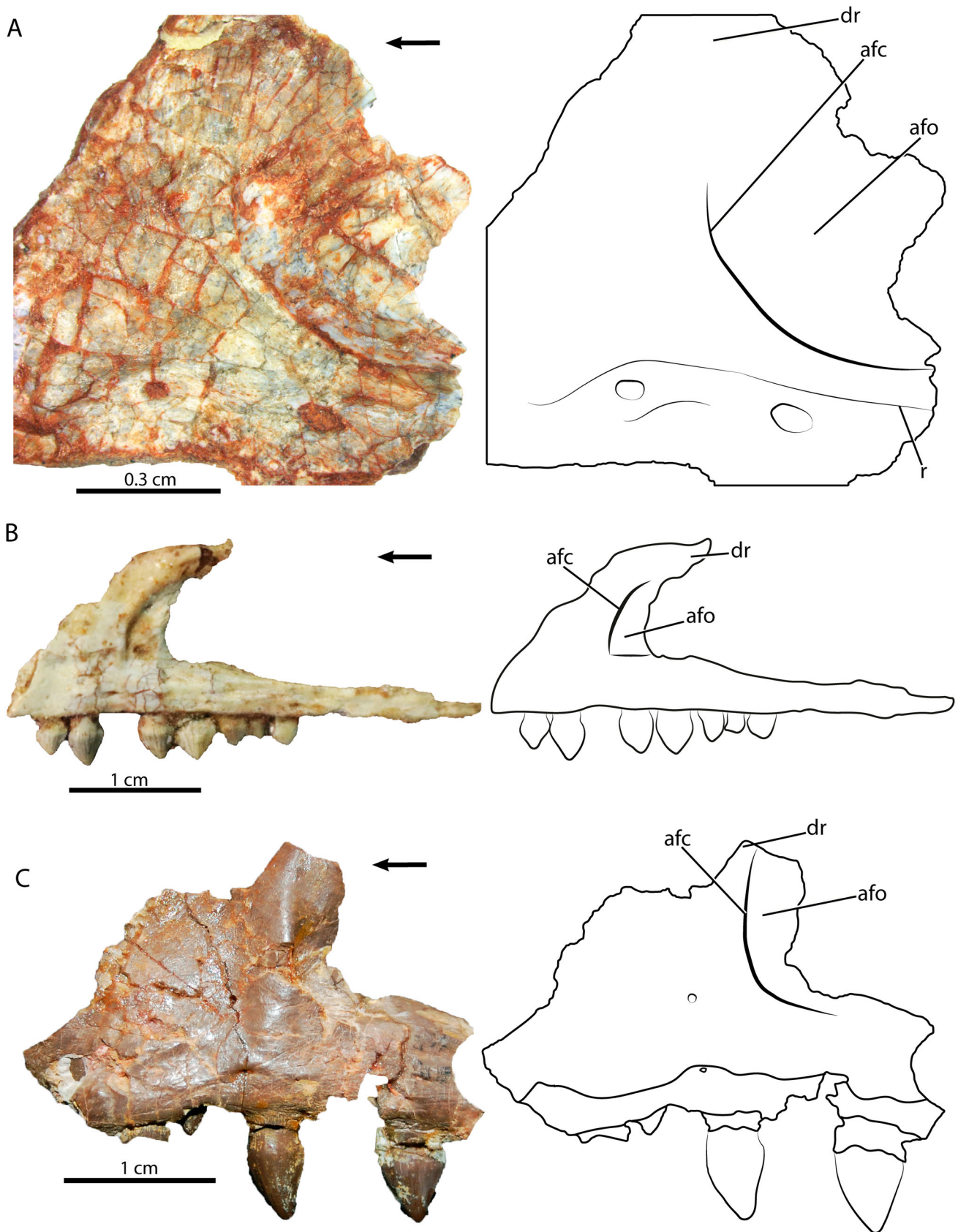


FIGURE 4. Comparison of the silesaurid antorbital fenestra. **A**, UFSM 11579A; **B**, *Sacisaurus agudoensis* (MCN PV10050); **C**, *Silesaurus opolensis* (ZPAL, Institute of Paleobiology of the Polish Academy of Sciences in Warsaw, Poland): B was purposely flipped (mirrored on Photoshop), so the three materials could face the same direction. **Abbreviations**: **afc**, crest of antorbital fenestra; **afo**, antorbital fossa; **dr**, dorsal margin. Arrows indicate the anterior direction.

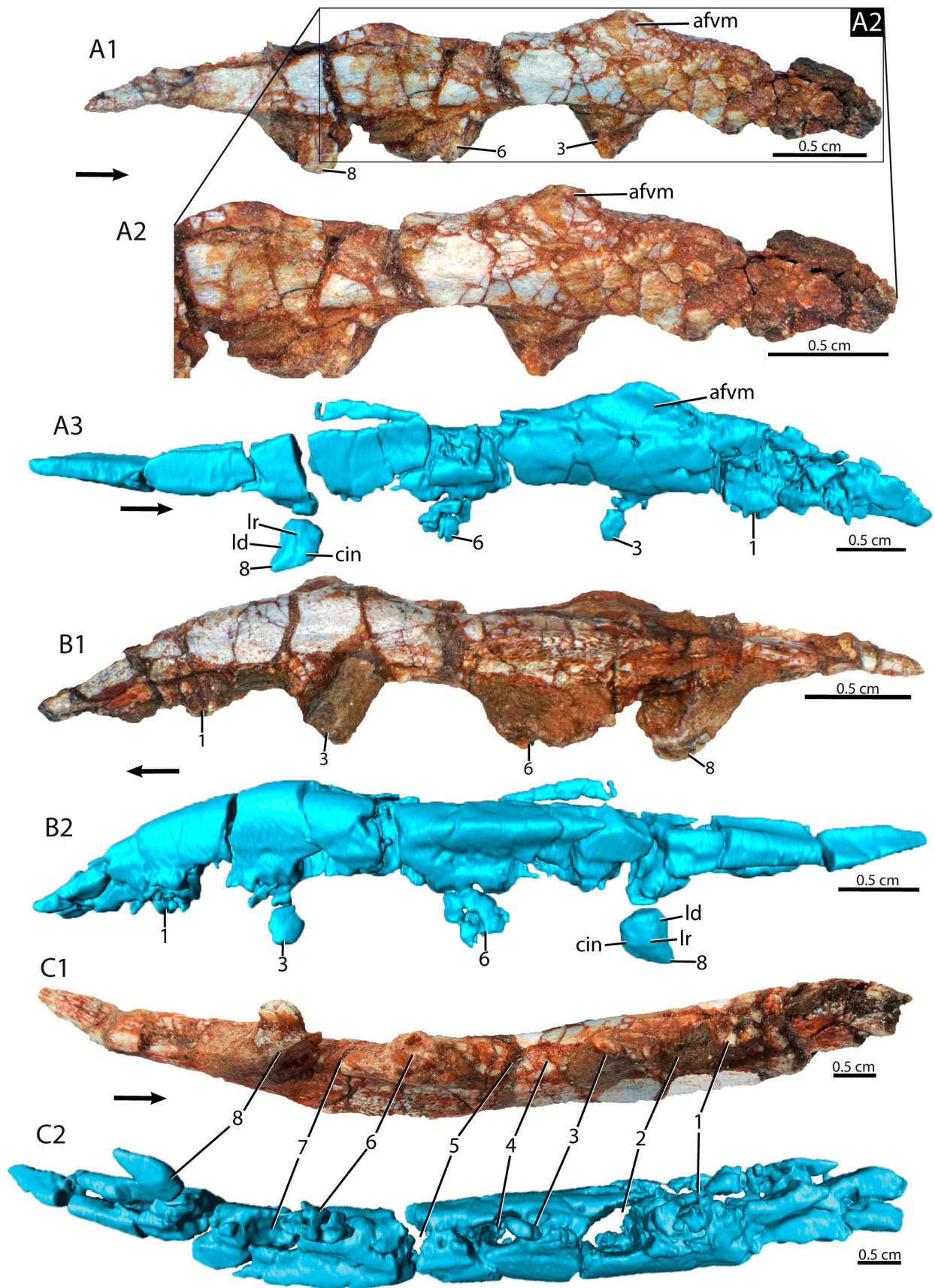


FIGURE 5. UFSM 11579B, right maxilla piece. **A1**, lateral view; **A2**, approximated view of the lateral view; **A3**, the digital image of the CT-scan segmentation, lateral view; **B1**, medial view; **B2**, the digital image of the CT-scan segmentation, medial view; **C1**, dorsal view; **C2**, the digital image of the CT-scan segmentation, dorsal view. **Abbreviations:** **afvm**, ventral margin of the anterior fenestra; **cin**, cingulum; **ld**, longitudinal depression; **lr**, longitudinal ridge. Numbers indicate the alveoli position from anterior to posterior.

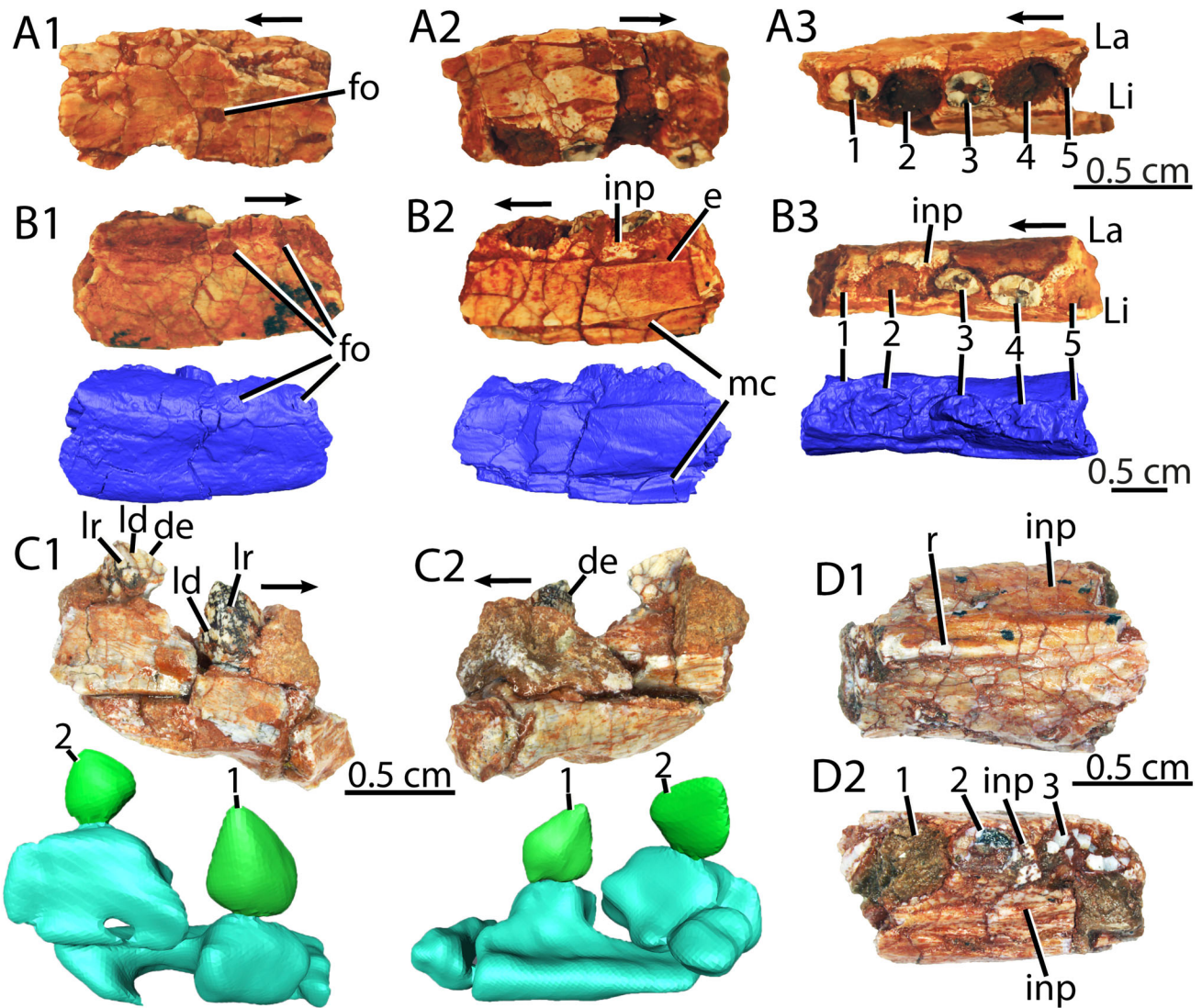


FIGURE 6. UFSM 11579. **A**, left maxilla piece (UFSM 11579C) in **A1**, lateral view; **A2**, medial view; **A3**, dorsal view. **B**, right lower jaw piece UFSM 11579D with a digitally reconstructed 3D model for each view: **B1**, lateral view; **B2**, medial view; **B3**, dorsal view. **C**, Right lower jaw piece UFSM 11579E with a digitally reconstructed 3D model for each view: **C1**, lateral view; **C2**, medial view. **D**, Lower jaw piece UFSM 11579F: **D1**, lateral/medial? view; **D2**, dorsal view. ‘A’ and ‘B’ were used in a previous Silesauridae tooth attachment survey (see Descriptions section), as can be found in Mestriner et al. (2022), Figures 5–9 and Supplementary Material, Figures S6 and S7. **Abbreviations:** **de**, denticles; **e**, edge; **fo**, foramen; **inp**, interdental plate; **La**, labial; **ld**, longitudinal depression; **Li**, lingual; **lr**, longitudinal ridge; **mc**, Meckelian canal; **r**, ridge. Numbers indicate the alveoli position, from the anterior to the posterior portion. Arrows indicate the anterior direction.

both the lingual and labial surfaces of the crown (Fig. 3B1, B2, C3, D, E). The ridges are flanked mesially and distally by longitudinal depressions, which more smoothly excavate the crown base (Fig. 3A, B1, B2, D, E3). This longitudinal ridge is similar to that seen in *Sacisaurus agudoensis* (see Langer & Ferigolo 2013:fig. 7F, K) and may correspond to the “central primary ridge” of some ornithischians (Butler et al., 2008).

Many denticles measuring on average 0.015 cm apicobasally and 0.020 cm mesiodistally are seen along both carinae of UFSM 11579A (Fig. 3B1, B2, D). Because the carinae are incomplete, it is not possible to define the exact number of denticles per side of the tooth, but it is possible to distinguish at least nine mesially and three distally (the distal carina is badly preserved, Fig. 3D). The tooth ends dorsally as a thin tip (Fig. 3B1, B2, C3, D), differing from the more rounded tooth tips of *Sacisaurus agudoensis*, *Silesaurus opolensis*, and *Diodorus scytobrachion* (Dzik, 2003; Langer & Ferigolo, 2013; Kammerer

et al., 2011). In general, UFSM 11579 seems to present a “foli-dont” tooth crown morphology (Fig. 3D), where the teeth are lanceolate instead of recurved, possess a midline ridge extending from the base to the apex on the lingual and labial surfaces, and have relatively large denticles projecting from the edges (sensu Hendrickx et al., 2015; Martz & Small, 2019). This is the same condition seen in *Sacisaurus agudoensis* and *Kwanasaurus williamparkeri*, but differs from those of *Asilisaurus kongwe*, *Lewisuchus admixtus*, and some specimens of *Silesaurus opolensis*, in which the teeth are either peg-like (Nesbitt et al., 2010, 2019), recurved (Ezcurra et al., 2019), or more conical (Dzik, 2003).

Even though the teeth of the right maxilla (UFSM 11579B) are damaged (Fig. 5), the 3D model (derived from CT data) allowed us to access the overall morphology of the eighth preserved tooth. It is generally like that of UFSM 11579A, but with a less protuberant cingulum, especially on the labial surface of the

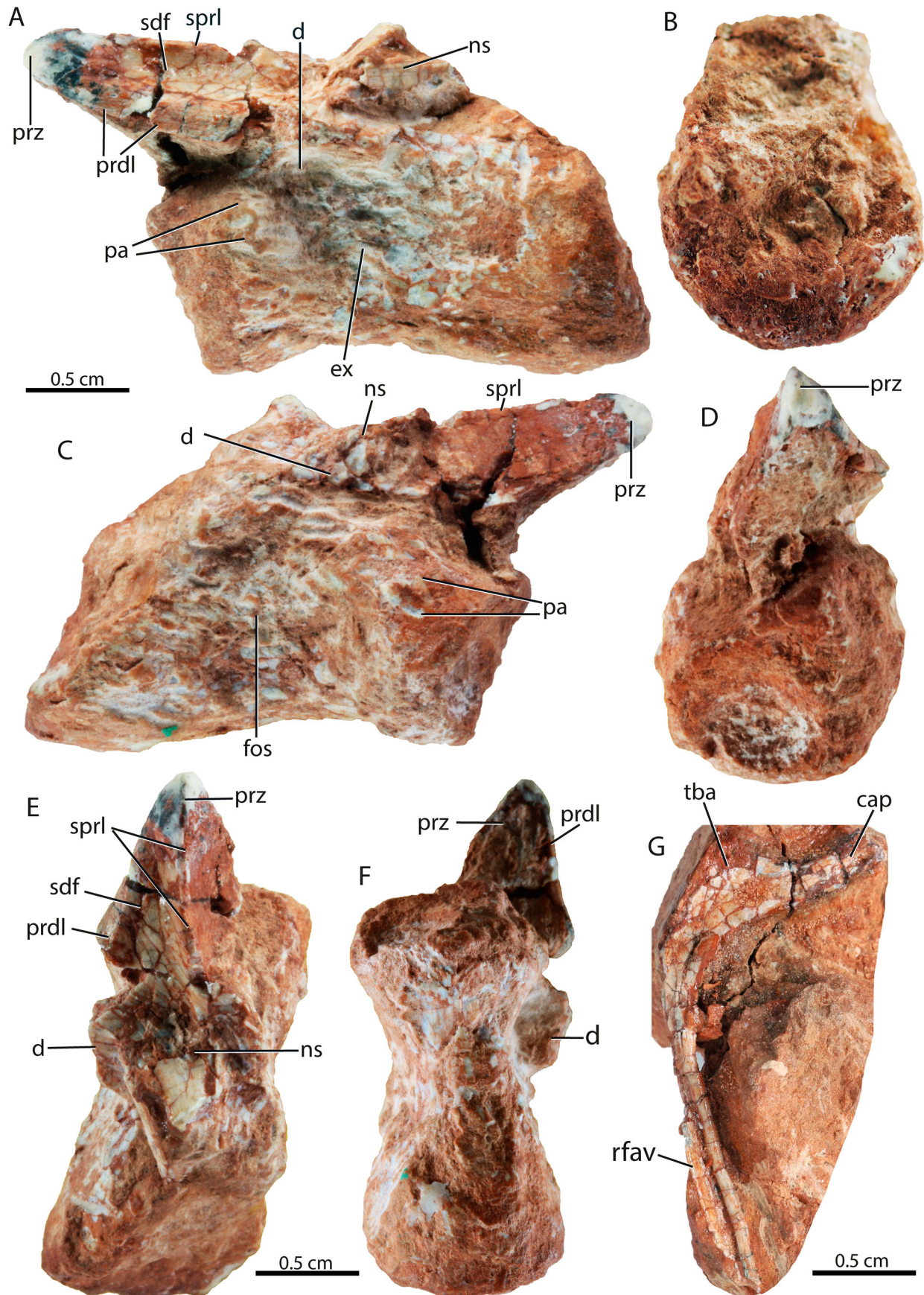


FIGURE 7. UFSM 11579G, cervical vertebra, and UFSM 11579G, cervical rib. **A**, lateral view; **B**, posterior view; **C**, the other lateral view; **D**, anterior view; **E**, dorsal view; **F**, ventral view; **G**, lateral view. **Abbreviations:** **cap**, capitulum; **d**, diapophysis; **ex**, excavation; **fos**, fossa; **ns**, neural spine; **pa**, parapophysis; **prdl**, prezygodiapophyseal lamina; **prz**, prezygapophysis; **rfav**, rib fragment of another vertebra; **sdf**, spinodiapophyseal fossae; **sprl**, spinoprezygapophyseal lamina; **tba**, tuberculum area.

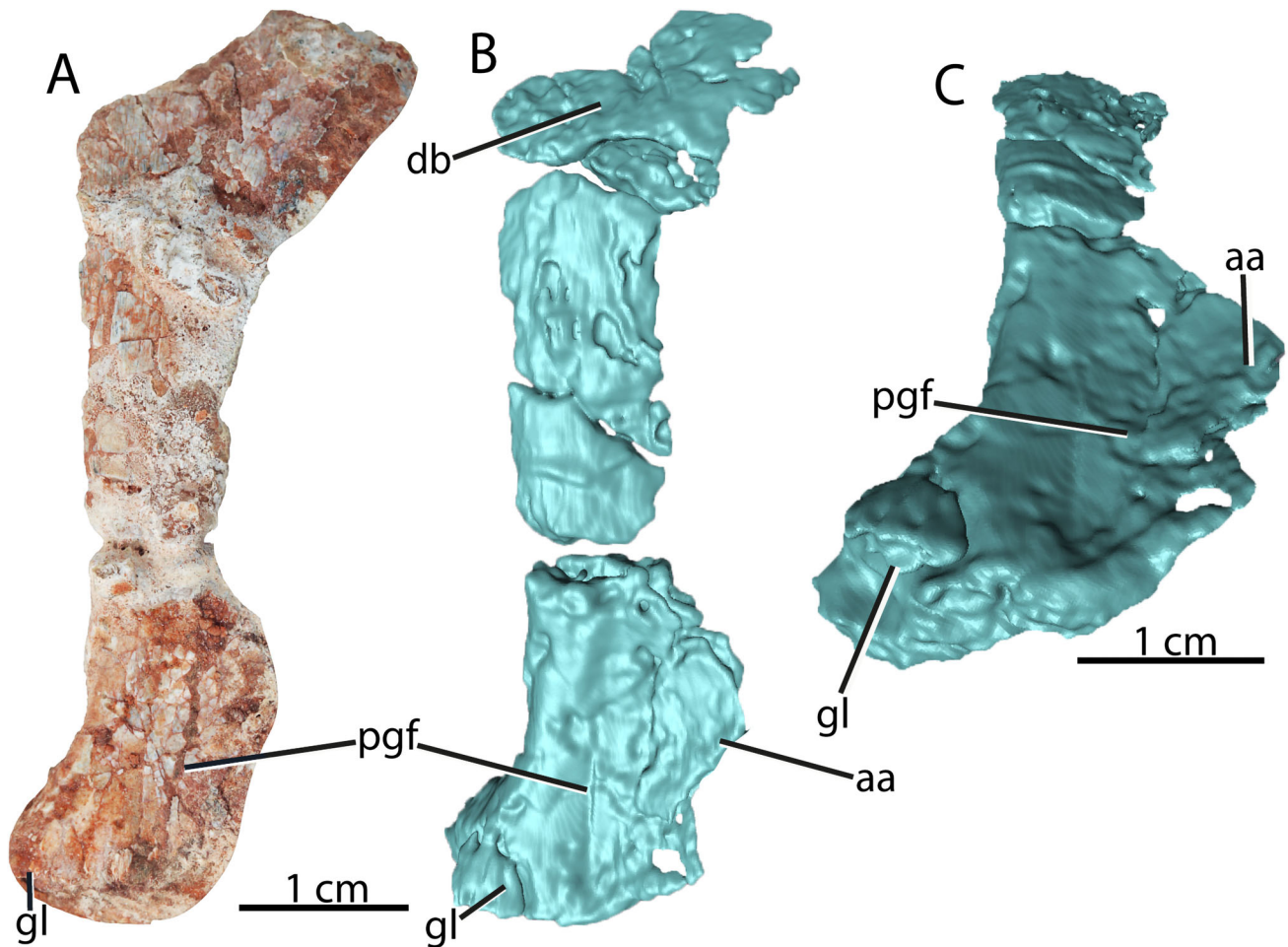


FIGURE 8. UFSM 11579I, right scapula. **A**, lateral view; **B**, digitally reconstructed lateral view. **Abbreviations:** **aa**, acromion area; **db**, dorsal blade; **gl**, glenoid; **pgf**, preglenoid fossa.

tooth (Fig. 5A3, B2). Its crown is also more posteriorly curved at the distal tip. Fully erupted teeth in the dentary are known only for UFSM 11579E (Fig. 6C). These are leaf-shaped like the maxillary teeth (Fig. 6E, F), but the lingual side is damaged, hampering the identification of a cingulum. The more posterior tooth is broken at its mesiobasal portion, whereas the other tooth is more complete. UFSM 11579E teeth (Fig. 6C) have at least seven denticles in both the mesial and distal carinae (damage precludes assessing their exact number), with sizes that do not differ from those of UFSM 11579A (ca. 0.015 cm apicobasally and 0.020 cm mesiodistally). The tooth has a smooth labial surface, as well as a longitudinal smooth depression excavating the crown base ('ld' in Fig. 6C1).

**Axial Skeleton**—An isolated partial cervical vertebra was recovered from the bone accumulation (UFSM 11579G; Fig. 7). It is not well-preserved, missing both postzygapophyses and most of the neural spine (Fig. 7A). Only the 1.2 cm long left prezygapophysis is preserved (Fig. 7C). The position of the diapophysis is inferred from the incomplete base on the left element, whereas the parapophysis corresponds to a low bump (Fig. 7). The centrum measures 2.2 cm in length and is parallelogram-shaped in lateral view (Fig. 7A, C), as in anterior cervical vertebrae of other early Pan-Aves (Nesbitt et al., 2019), with the anterior articular facet placed dorsal to the posterior (Fig. 7A, C). The lateral surface of the centrum possesses a shallow and poorly defined anteroposteriorly elongated excavation (Fig. 7A).

The ventral surface of the centrum is badly preserved, but seems to lack the ventral keel (Fig. 7F) seen in some silesaurids (Nesbitt et al., 2019), such as *Asilisaurus kongwe* (Nesbitt et al., 2010, 2019) and *Silesaurus opolensis* (ZPAL Ab III/unnumbered—Nesbitt et al., 2019). The anterior and posterior articular facets are both slightly concave (Fig. 7B, D). The prezygapophysis projects beyond the anterior rim of the centrum (Fig. 7A, C, E, F) and two distinct laminae extend along its dorsal and lateral surfaces. Laterally, the prezygodiapophyseal lamina (prdl—Wilson 1999; Wilson et al., 2011) extends anterodorsally from the diapophysis toward the tip of the prezygapophysis, flanking this structure laterally (Fig. 7A). More dorsally, the spinoprezygapophyseal lamina (sprl—Wilson 1999; Wilson et al., 2011) extends along the prezygapophysis dorsal surface to meet the anterior end of the broken neural spine (Fig. 7A, C). The area between both laminae is well marked by the spinodiapophyseal fossa (sdf—Wilson et al., 2011).

An incomplete cervical rib was recovered from the bone accumulation (UFSM 11579H). It is badly preserved, with the material still associated to the matrix (Fig. 7G). The rib is slender, proximally bifurcated into capitulum and tuberculum, the latter of which is missing. The former is rounded and forms a 90° angle to the shaft. The narrower and rod-like shaft is distally incomplete, so that its length cannot be assessed. The shaft curves gently from the point where the tuberculum and capitulum diverge, and it is nearly straight distal to that. A piece of another rib was preserved next to that shaft (Fig. 7G).

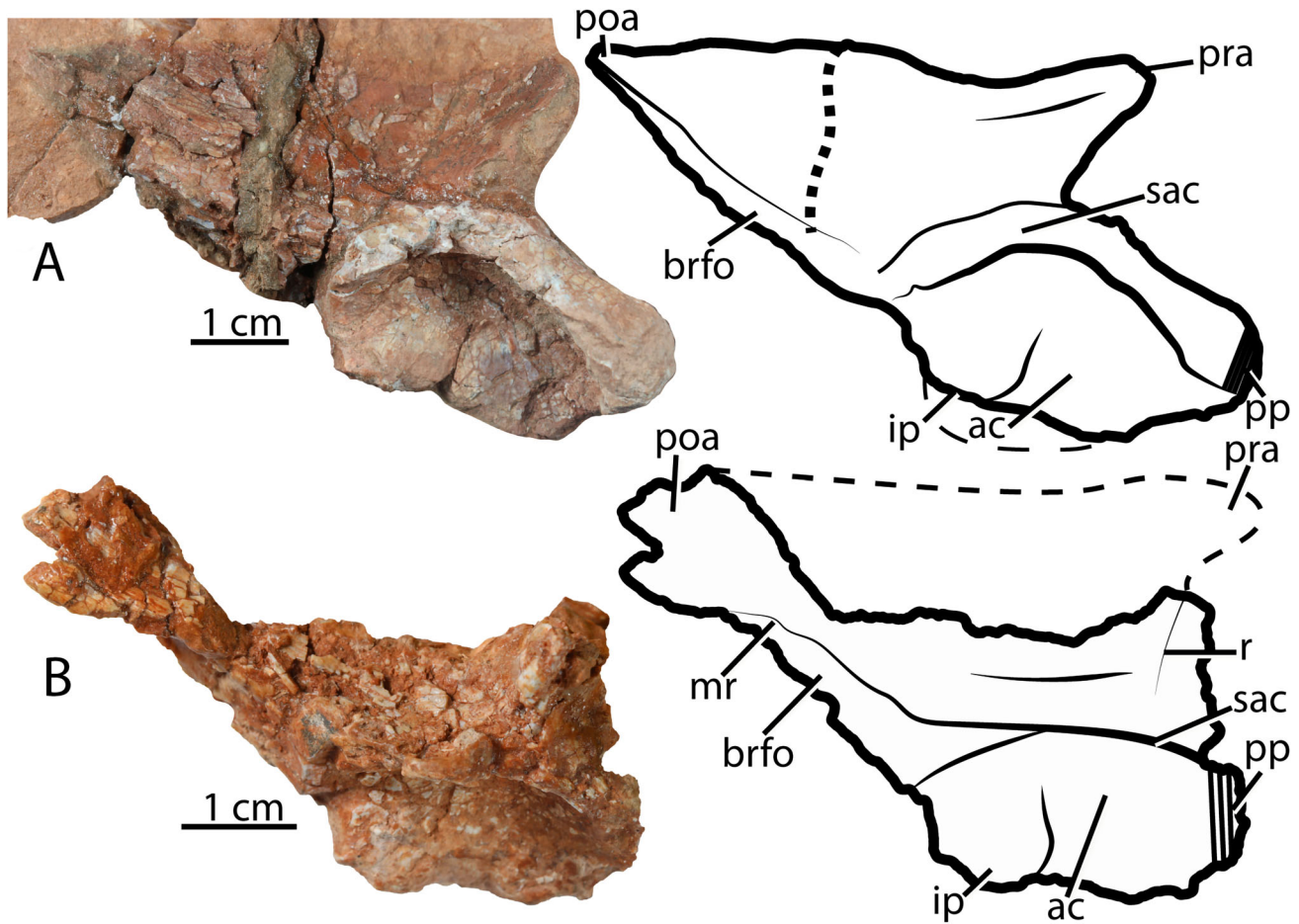


FIGURE 9. Two right ilia: **A**, UFSM 11579J in lateral view; **B**, UFSM 11579 K in lateral view. **Abbreviations:** **ac**, acetabulum; **brfo**, brevis fossa; **ip**, ischiadic peduncle; **mr**, medial ridge; **poa**, postacetabular ala; **pp**, pubic peduncle; **pra**, preacetabular ala; **r**, ridge; **sac**, supracetabular crest. Dashed area indicates the missing portion of the ilium.

**Scapula**—An isolated, incomplete, and damaged right scapula is the only recovered element of the pectoral girdle (UFSM 1579I; Fig. 8). It is partially embedded in the matrix and exposed in lateral view (Fig. 8). The scapula measures 5.5 cm dorsoventrally and is mediolaterally flattened, bowing medially at its dorsal portion. The posterior margin of the blade is straight, but the anterior gradually projects anteriorly towards its dorsal margin. As in *Sacisaurus agudoensis* (Langer & Ferigolo, 2013), the scapular blade reaches its minimal and maximal anteroposterior width respectively near the base (0.7 cm) and at the dorsal margin. The dorsal expansion coupled with the well-developed acromion, confers to the anterior margin of the blade a concave aspect. The glenoid is posteroventrally and slightly laterally oriented, forming an angle of approximately 45° in lateral view respective to the scapular main axis. On the lateral surface, a subtle preglenoid fossa is present between the glenoid and the acromion area, resembling the condition in early pan-avians, such as *Silesaurus opolensis* (Dzik, 2003), *Sacisaurus agudoensis* (Ferigolo & Langer, 2007), and *Teleocrater rhadinus* (Nesbitt et al., 2017b). The distal end surface is nearly flat, and thicker posteriorly than anteriorly, resembling the condition in *Silesaurus opolensis* (Dzik, 2003), *Sacisaurus agudoensis* (Langer & Ferigolo, 2013), and *Teleocrater rhadinus* (Nesbitt et al., 2017a, 2017b).

**Ilium**—Two isolated and incomplete right ilia are preserved (Fig. 9). The more complete element is only exposed laterally (11579J; Fig. 9A), given that its medial side is still embedded in

matrix. Its maximum anteroposterior length is 7.0 cm, whereas the maximum dorsoventral height is 3.5 cm. Most of the iliac blade, including the pre- and postacetabular alae are only accessible by their impressions in the rock matrix. The other ilium is mostly represented by its acetabular region and brevis fossa (UFSM 11579 K; Fig. 9B).

The preacetabular ala is subtriangular in lateral view and does not extend anterior to the pubic peduncle (Fig. 9A). Its anterior portion is gently rounded and arches laterally as it extends anteriorly. The acetabular antitrochanter is set at the posteroventral corner of the acetabulum, as a planar and barely differentiated surface (Fig. 9). The anterior edge of the acetabular medial wall merges with the posteromedial portion of the pubic peduncle, which is 2.2 cm long, has a columnar aspect and an anteroventrally facing articulation for the pubis (Fig. 9A). There is a subtle ridge extending from the middle of the supraacetabular crest to the lateral edge of the preacetabular ala (Fig. 9B), which is also seen in *Asilisaurus kongwe* (Nesbitt et al., 2019: fig. 36A, labeled “r”). The ischiadic peduncle is continuous with the distal portion of the acetabular wall and it is mainly vertical in lateral view.

The supraacetabular crest is missing in both ilia, but its position is indicated by the outline of its base (Fig. 9). It lies in the middle of the dorsoventral height of the ilium and covers the entire anteroposterior extent of the acetabulum. Even though breakages hamper evaluation of its shape, the supraacetabular crest of UFSM 11579 K (‘sac’ in Fig. 9B) is gently projected ventrally.

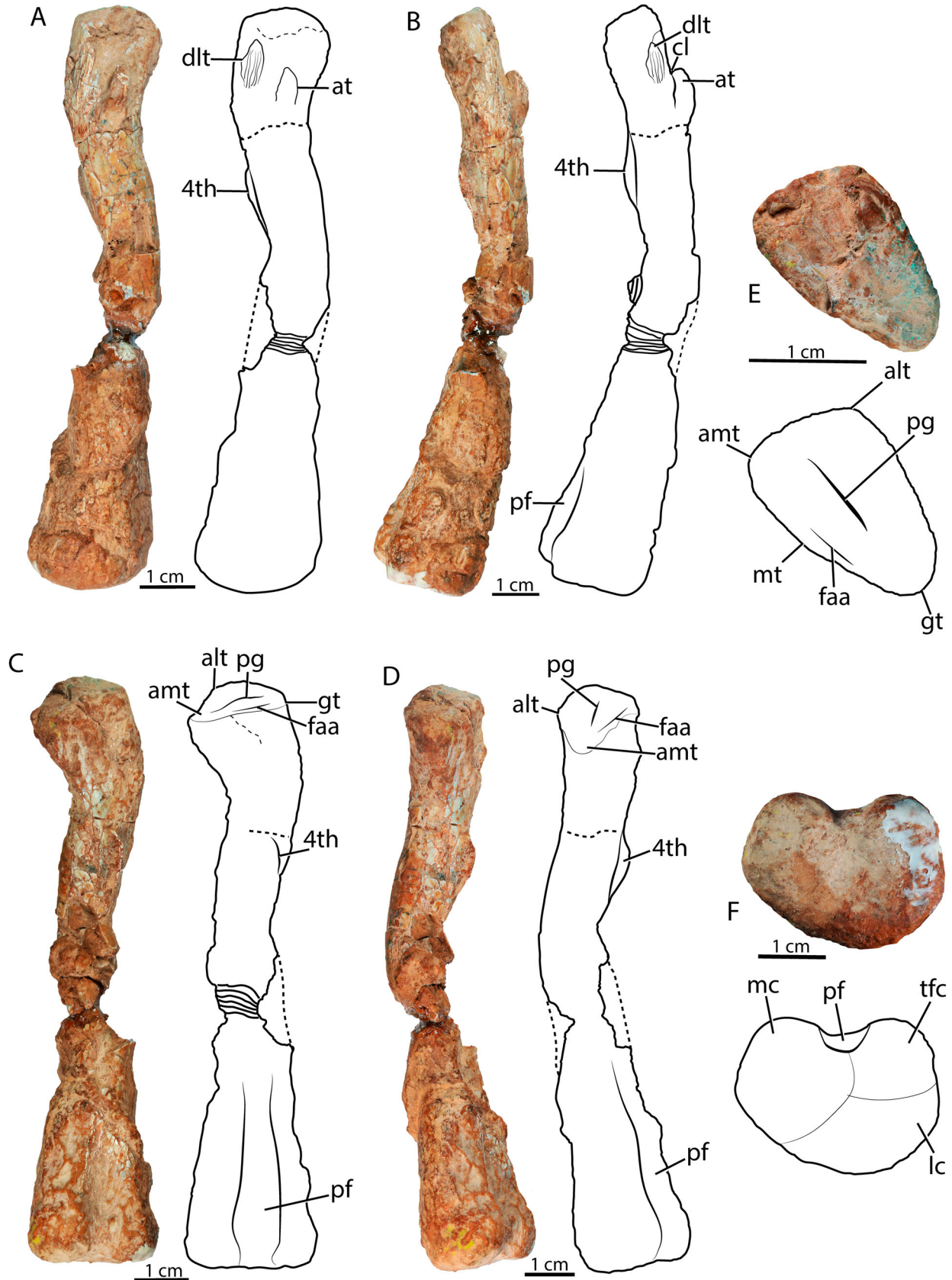


FIGURE 10. UFSM 11579L, right femur: **A**, anterior view; **B**, lateral view; **C**, posterior view; **D**, medial view; **E**, proximal view; **F**, distal view. **Abbreviations:** **alt**, anterolateral tuber; **amt**, anteromedial tuber; **at**, anterior trochanter; **cl**, cleft; **dlt**, dorsolateral trochanter; **faa**, facies articularis antitrochanterica; **gt**, great trochanter; **lc**, lateral condyle; **mc**, medial condyle; **mt**, medial tuber; **pf**, popliteal fossa; **pg**, proximal groove; **tfc**, tibiofibular condyle; **4th**, fourth trochanter.

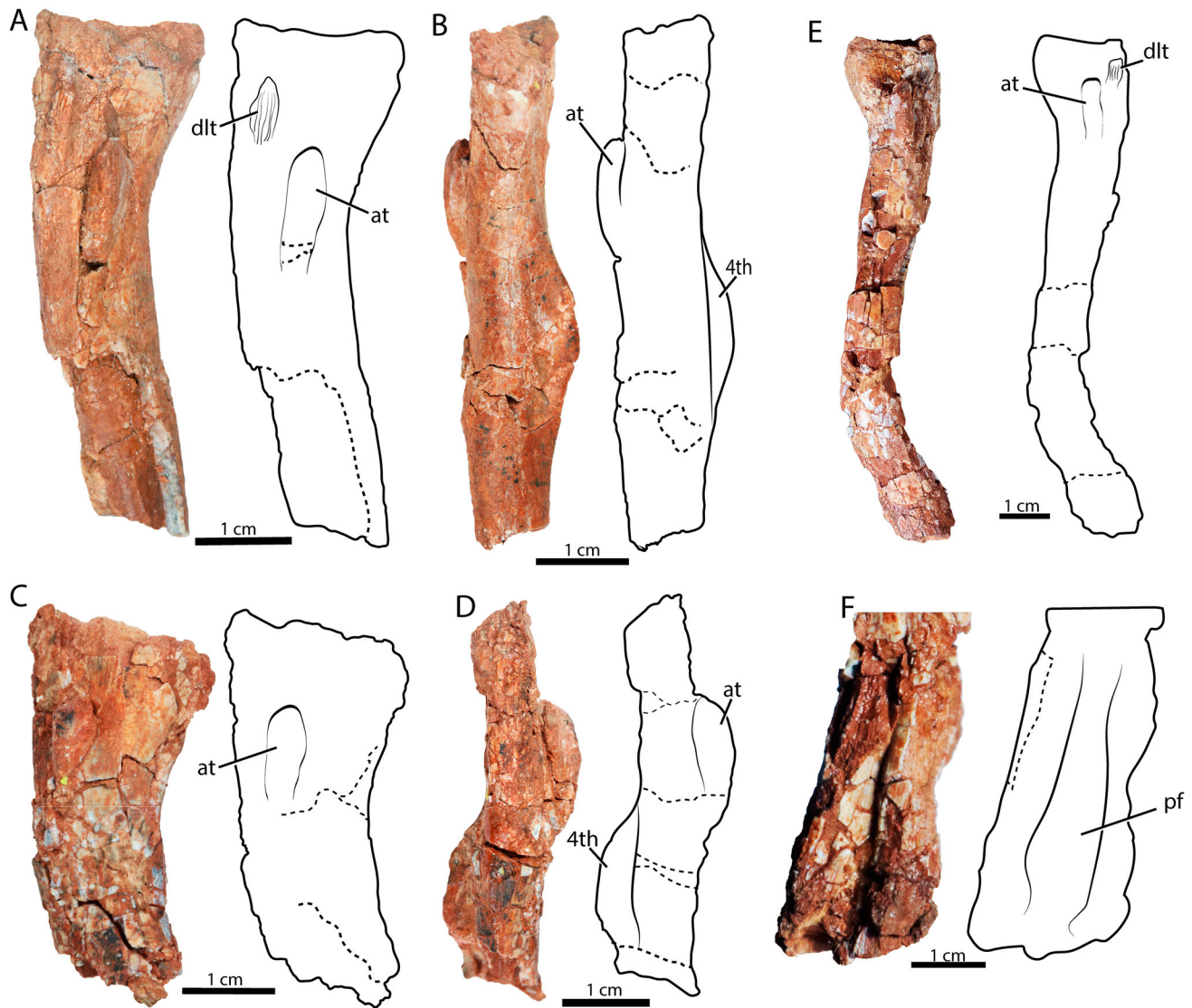


FIGURE 11. UFSM 11579M, right femur: **A**, anterior view; **B**, medial view. UFSM 11579N, right femur: **C**, anterior view; **D**, lateral view. UFSM 11579O, left femur: **E**, anterior view; **F**, close-up on its posterodistal portion showing the well-excavated popliteal fossa. **Abbreviations:** at, anterior trochanter; dlt, dorsolateral trochanter; pf, popliteal fossa; 4th, fourth trochanter.

The ventral margin of the ilium is convex, with the acetabular medial wall closing the entire iliac acetabulum (Fig. 9A), as typical for most non-dinosaurian archosaurs (Gauthier, 1986; Langer & Benton, 2006; Nesbitt, 2011), including silesaurids (Dzik, 2003; Ezcurra et al., 2019; Langer & Ferigolo, 2013; Martínez et al., 2011; Nesbitt, 2011; Nesbitt et al., 2019; Peacock et al., 2013). The acetabulum is anteroposteriorly longer (2.7 cm) than dorsoventrally tall (1.5 cm), the ventral margin of the medial wall is subtriangular and extends ventral to the pubic and ischiadic peduncles, resembling the condition of *Asilisaurus kongwe* (Nesbitt et al., 2019).

The postacetabular ala bears an anteroposteriorly elongated and ventrally oriented subtriangular fossa, with 0.9 cm of maximal width, the lateral margin of which extends as a ridge that connects to the supracetabular crest (Fig. 9B). This corresponds to the brevis fossa (Langer & Benton, 2006; Novas, 1996), which also occurs in several dinosauriforms such as *Lewisuchus admixtus* (Ezcurra et al., 2019), *Asilisaurus kongwe* (Nesbitt et al., 2019), *Silesaurus opolensis* (ZPAL Ab III/907/8, 404/1), *Sacisaurus agudoensis* (Langer & Ferigolo, 2013),

*Lutungutali sitwensis* (Peacock et al., 2013), *Eucoelophysis baldwini* (GR 225), and *Ignotosaurus fragilis* (Martínez et al., 2012). In contrast, some other pan-avians such as *Lagerpeton chanarensis*, *Ixalerpeton polesinensis*, and *Lagosuchus lilloensis*, lack such a fossa (Ezcurra et al., 2019; Novas, 1996; Sereno & Arcucci, 1994). A ridge extends anteroposteriorly flanking the brevis fossa laterally (Fig. 9B), forming the ventral margin of the posterior portion of the postacetabular ala, where the fossa is partially exposed laterally. This differs from the condition of the silesaurids *Lutungutali sitwensis* (Peacock et al., 2013), *Sacisaurus agudoensis* (Langer & Ferigolo, 2013), *Silesaurus opolensis* (Dzik, 2003), and a specimen referred to *Lewisuchus admixtus* (CRILAR-Pv 552), in which the fossa is more laterally directed.

**Femur**—Three right (UFSM 11579L-N; Figs. 10, 11A–D) and three left (UFSM 11579O–Q; Figs. 11E, F, 12) femora are preserved, most of them fragmentary. The two more complete femora are 10.0 and 11.2 cm long (Figs. 10, 11E; Table 1). All femora are nearly identical, although taphonomic distortions modified their overall shape in some parts, especially the



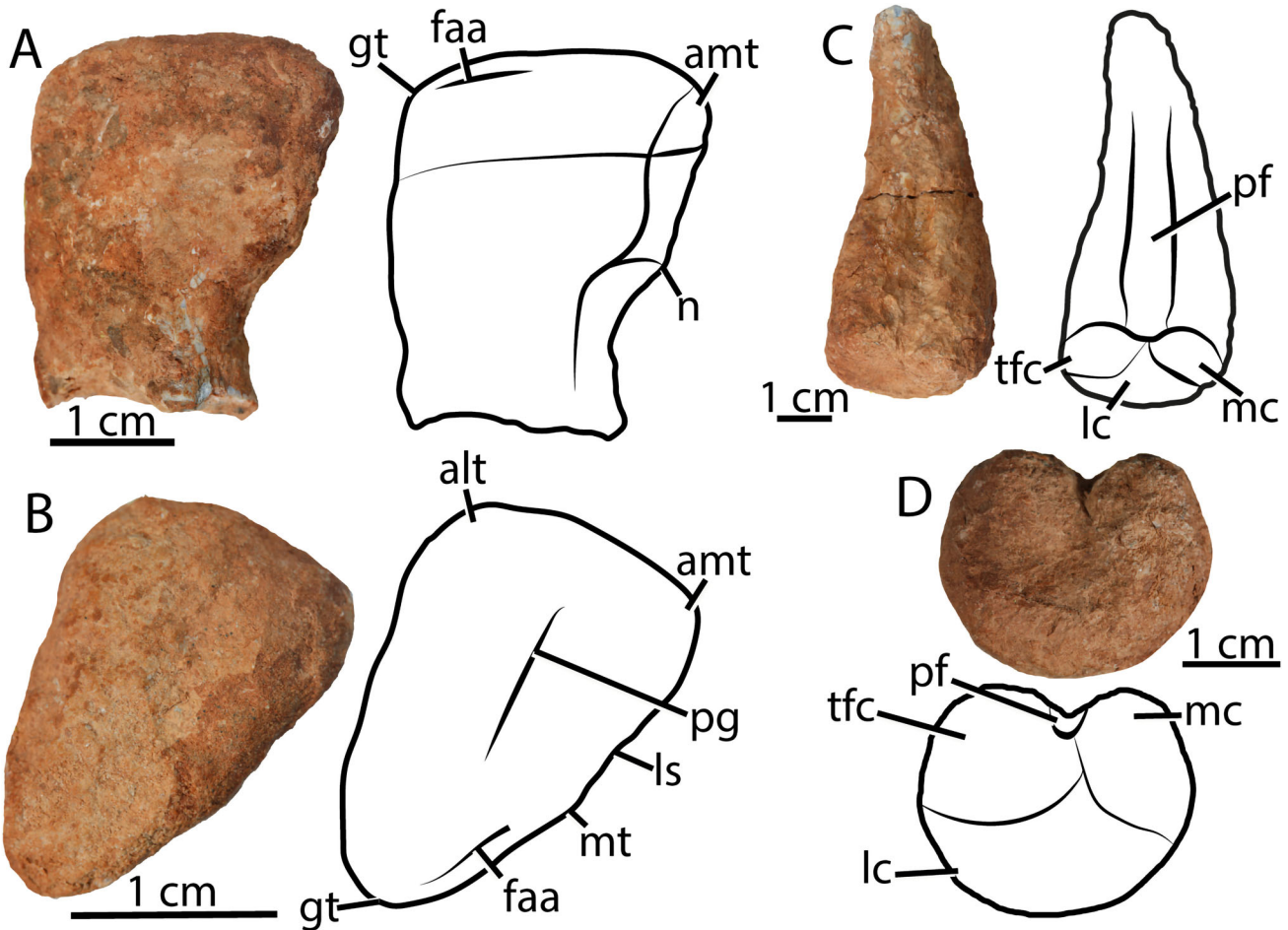


FIGURE 12. UFSM 11579P, left proximal femur: **A**, posterior view; **B**, proximal view. UFSM 11579Q, left distal femur: **C**, posterior view; **D**, distal view. **Abbreviations:** alt, anterolateral tuber; amt, anteromedial tuber; faa, facies articularis antitrochanterica; gt, great trochanter; lc, lateral condyle; ls, ligament sulcus; mc, medial condyle; mt, medial tuber; n, notch; pf, popliteal fossa; pg, proximal groove; tfc, tibiofibular condyle.

proximal and distal articulations. The bone is sigmoid in lateral/medial views, given the medial and lateral curvatures of its proximal and distal portions (Figs. 10–12). The proximal outline of the femoral head is subtriangular, with clear anteromedial and anterolateral tubera (Figs. 10C–E, 12B). Its maximum lateromedial width varies from 1.8–2.3 cm and the anteroposterior length from 0.6–1.2 cm (see Table 1). The anterior margin of the femoral head, connecting the anterolateral and anteromedial tubera, is flat, forming part of the triangular shaped head typical of Silesauridae (Dzik, 2003; Ferigolo & Langer, 2007; Kammerer et al., 2011; Langer & Ferigolo, 2013; Müller & Garcia, 2023; Nesbitt, 2011; Nesbitt et al., 2019). This condition differs from that of most archosauriforms, in which the femur has a rounded anterior margin in proximal view (Nesbitt, 2011). The anteromedial tuber is not as developed as that of most early dinosaurs, e.g., *Nhandumirim waldsangae*, *Saurnalia tupiniquim* (Langer, 2003; Marsola et al., 2019a), but it is rounded, medially projected, and larger than the medial tuber, as seen in *Sacisaurus agudoensis*, *Asilisaurus kongwe*, and early dinosaurs (Langer, 2003; Langer & Ferigolo, 2013; Marsola et al., 2019a; Nesbitt et al., 2019). The medial tuber is low and rounded, occupying less than one-third of the medial edge of the femoral head. The “ligament sulcus” (Novas, 1996) is very subtle and separates the anteromedial and medial tubera (Fig. 12B), differing from the better developed excavation seen in

several *Sacisaurus agudoensis* individuals (see Langer & Ferigolo, 2013:fig. 16A, B). The elevated profile of the posterior corner of the femoral head is given by the “great trochanter,” which forms a nearly right angle in posterior view. Additionally, its posteromedial edge forms the ‘facies articularis antitrochanterica,’ which is not depressed, as also seen in *Sacisaurus agudoensis* and *Silesaurus opolensis* (Dzik, 2003; Langer & Ferigolo, 2013). In proximal view, the femur bears a distinct and straight groove (Figs. 10E, 12B).

There is a notch distal to the anteromedial projection of the femoral head, as better seen in UFSM 11579P (Fig. 12A) and considered typical of silesaurids (Irmis et al., 2007; Kammerer et al., 2011; Langer & Ferigolo, 2013; Nesbitt et al., 2010). Indeed, the distal margin of the UFSM 11579P femoral head does not form a distally continuous curve, as in lagerpetids (Nesbitt et al., 2009) and *Lagosuchus lilloensis* (PVL 3870), but it is instead angled relative to the shaft, as in silesaurids and dinosaurs (Langer & Benton, 2006; Langer & Ferigolo, 2013). Also, the femoral head is not medially expanded as in those lagerpetids and dinosaurs, better matching the typical silesaurid condition (Dzik, 2003; Ezcurra, 2006; Irmis et al., 2007; Kammerer et al., 2011; Nesbitt et al., 2007, 2010).

The dorsolateral trochanter is proximodistally elongated and does not reach the proximal margin of the femur. It is located slightly proximal to the anterior trochanter, matching the position

and morphology commonly found in early dinosauriforms (Langer & Benton, 2006; Novas, 1996), such as silesaurids (Dzik, 2003; Ferigolo & Langer 2007; Nesbitt et al., 2019) and the dinosaur *Nhandumirim waldsangae* (Marsola et al., 2019a). On the other hand, the dorsolateral trochanter of most other early dinosaurs is positioned well proximal to the level of the anterior trochanter (Figs. 10A, 11A, E), e.g., *Saturnalia tupiniquim* (Langer, 2003), *Liliensternus liliensterni* (Langer & Benton, 2006; Nesbitt, 2011), *Staurikosaurus pricei* (Bittencourt & Kellner, 2009). As in *Sacisaurus agudoensis*, the dorsolateral trochanter is crenulated and scarred, revealing muscle insertion sites. The anterior trochanter is prominent (see Table 1 for measurements), positioned anterior to the dorsolateral trochanter. In UFSM 11579L-O, it is ovoid in cross section, with the spike-like morphology (Figs. 10A, B, 11) typical of silesaurids (Dzik, 2003; Langer & Ferigolo, 2013; Nesbitt, 2011), such as *Silesaurus opolensis* (Dzik, 2003), *Sacisaurus agudoensis* (Ferigolo & Langer, 2007; Langer & Ferigolo, 2013), *Diodorus scytobrachion* (Kammerer et al., 2011), *Eucoelophysys baldwini* (Sullivan & Lucas, 1999), *Lewisuchus admixtus* (Ezcurra et al., 2019), and *Amanasaurus nesbitti* (Müller & Garcia, 2023). It is also proximodistally striated and projected laterally from the femoral shaft, differing from the more subtle anterior trochanter of *Asilisaurus kongwe* (Nesbitt et al., 2019) and some early dinosaurs (e.g., *Saturnalia tupiniquim*, *Nhandumirim waldsangae*; Langer, 2003; Marsola et al., 2019a). The proximal portion of the anterior trochanter of UFSM 11579L-O is separated from the shaft by a subtle cleft. This condition is found more pronounced in *Sacisaurus agudoensis* (Langer & Ferigolo, 2013:fig. 16E).

The fourth trochanter is located at the posteromedial portion of the proximal third of the femur (Figs. 10, 11B, D). It is symmetric proximodistally, as for other non-dinosaur dinosauriforms (Ezcurra et al., 2019; Nesbitt et al., 2010; Nesbitt, 2011), forming obtuse angles to the shaft. The UFSM 11579L-O fourth trochanter (Figs. 10, 11) is not as expanded as that of *Lewisuchus admixtus* (Ezcurra et al., 2019), resembling more the condition of other silesaurids such as *Sacisaurus agudoensis* (Ferigolo & Langer, 2007; Langer & Ferigolo, 2013), *Silesaurus opolensis* (Dzik, 2003), *Eucoelophysys baldwini* (Sullivan & Lucas, 1999), and *Asilisaurus kongwe* (Griffin & Nesbitt, 2016; Nesbitt et al., 2019). Medial to the fourth trochanter, a proximodistally elongated scar marks the attachment of *M. caudofemoralis longus* (Langer & Ferigolo, 2013).

The anatomy of the distal end of the femur can be partially accessed via the preserved parts of UFSM11579 L, O, and N (Figs. 10C, D, F, 11F, 12C, D). The bone gradually expands toward the distal end (Fig. 10C; Table 1), the posterior surface of which seems to lack the proximodistally oriented “caudomedial groove” and the “caudomedial ridge” seen in *Sacisaurus agudoensis* (Langer & Ferigolo, 2013:figs. 12C, 17I), but bears a proximodistally oriented and well-developed popliteal fossa (Yates, 2003), or “intercondylar groove” (Butler, 2010). It extends for the whole distal third of the femur (Figs. 10C, D, F, 11F, 12C, D), a condition shared among silesaurids, such as *Sacisaurus agudoensis* (Langer & Ferigolo, 2013), *Diodorus scytobrachion* (Kammerer et al., 2011), and *Silesaurus opolensis* (Dzik, 2003).

The distal outline of the femur is rounded and lateromedially broader than anteroposteriorly long (Figs. 10F, 12D). The tibiofibular crest (lateral condyle of Langer & Ferigolo, 2013) is posterolaterally pointed and continuous with the lateral condyle (fibular condyle of Langer & Ferigolo, 2013). The lateral condyle has its anterior margin subtly more convex than the medial condyle, whereas the tibiofibular crest is subtly more posteriorly extended than the medial condyle (Figs. 10F, 12D). The lateral condyle and the tibiofibular crest are separated by a shallow cleft that culminates in a central fossa.

**Tibia**—Two incomplete and damaged left tibiae were recovered, one represented only by the proximal end (UFSM 11579R; Fig. 13A) and a more complete one missing only its distal end (UFSM 11579S; Fig. 13B). The proximal outline of the bone has a convex medial margin, whereas the lateral margin is concave. The medial condyle is more posteriorly extended than the fibular condyle, as in other non-dinosaur dinosauriforms (*Lagosuchus lilloensis*, Sereno & Arcucci, 1994; *Lewisuchus admixtus*, Ezcurra et al., 2019), sauropodomorphs (*Saturnalia tupiniquim* MCP 3845-PV), and ornithischians (e.g., *Lesothosaurus diagnosticus*, NHMUK PV RU B17; Baron et al., 2017b). This contrasts with the condition of neotheropods, in which the two condyles are located at the same level at the posterior margin (Ezcurra et al., 2019; Langer & Benton, 2006). The separation of the two condyles is not clear because of poor preservation.

A medially kinked and straight cnemial crest is present (Fig. 13A3, B3), although it is not as pronounced as in various early dinosaurs, e.g., *Heterodontosaurus tucki* (Luca & Luca, 1980), *Herrerasaurus ischigualastensis* (Novas, 1994), *Saturnalia tupiniquim* (Langer, 2003), and *Dilophosaurus wetherilli* (Tykoski, 2005). Instead, it is more like the cnemial crest of many silesaurids such as *Asilisaurus kongwe* (Nesbitt et al., 2010, 2019), *Lewisuchus admixtus* (Ezcurra et al., 2019), *Sacisaurus agudoensis* (Langer & Ferigolo, 2013), and *Silesaurus opolensis* (Dzik, 2003). The proximalmost portion of the lateral surface of the tibia has a proximodistally extended excavation, which seems to be related to the reception of the fibular head (Fig. 13A1, B1). The tibial shaft is nearly straight (Fig. 15B), lateromedially flattened proximally, but gradually turning more ovoid towards the distal portion.

**Fibula**—Two proximal portions of left fibulae were recovered (UFSM 11579T-U; Fig. 13C, D), both very damaged and dissociated from the tibiae. UFSM 11579 T is sigmoidal in lateral/medial views (Fig. 13C), whereas UFSM 11579U is thinner and straighter. Both are less robust than the tibia and UFSM 11579 T bears an anteroposteriorly expanded proximal end. Both fibulae are mediolaterally compressed, generally three times anteroposteriorly longer than mediolaterally wide in cross section (Table 1). The proximal end of UFSM11579U is medially bowed, anteriorly expanded, and more than twice wider than the shaft, whereas that of UFSM 11579U is straight, not expanded, and has the same thickness of its shaft. They bear a proximodistally oriented scar on the medial face (Fig. 13C1), as in *Silesaurus opolensis* (Dzik 2003—specimen ZPAL Ab III-361 and 362).

**Pedal Phalanx**—The pedal digits are represented only by one non-ungual phalanx (UFSM11579V; Fig. 14). Even though the phalanx is not articulated, it is tentatively associated to the right fourth phalanx of the fourth digit, based on a direct comparison with the pes of *Nhandumirim waldsangae* (Marsola et al., 2019a). The proximal articulation is about as high as wide and has a very subtle ventral ridge (Fig. 14E) separating the concave articular surface into a broader medial and a smaller lateral facet. The difference in size between the two condyles (lateral and medial) seems to be related to the lateral displacement of the phalanx/digit.

The phalanx is proximodistally elongated (maximum length of 2.21 cm), with a distinctly concave proximal surface (Fig. 14C). Both ventral and dorsal “proximal intercondylar processes” are well developed, with a waning crescent moon aspect in lateral and medial views (Fig. 14A, B). As in *Sacisaurus agudoensis* (Langer & Ferigolo, 2013), the ventral intercondylar process is twice longer than the dorsal (Fig. 14A–C). The proximal half of the ventral surface is flattened for the insertion of the flexor ligament. The ventral area separating the proximal half from the distal articulation of the phalanx is delimited by an extensive excavation (Fig. 14D). This region marks the middle of the

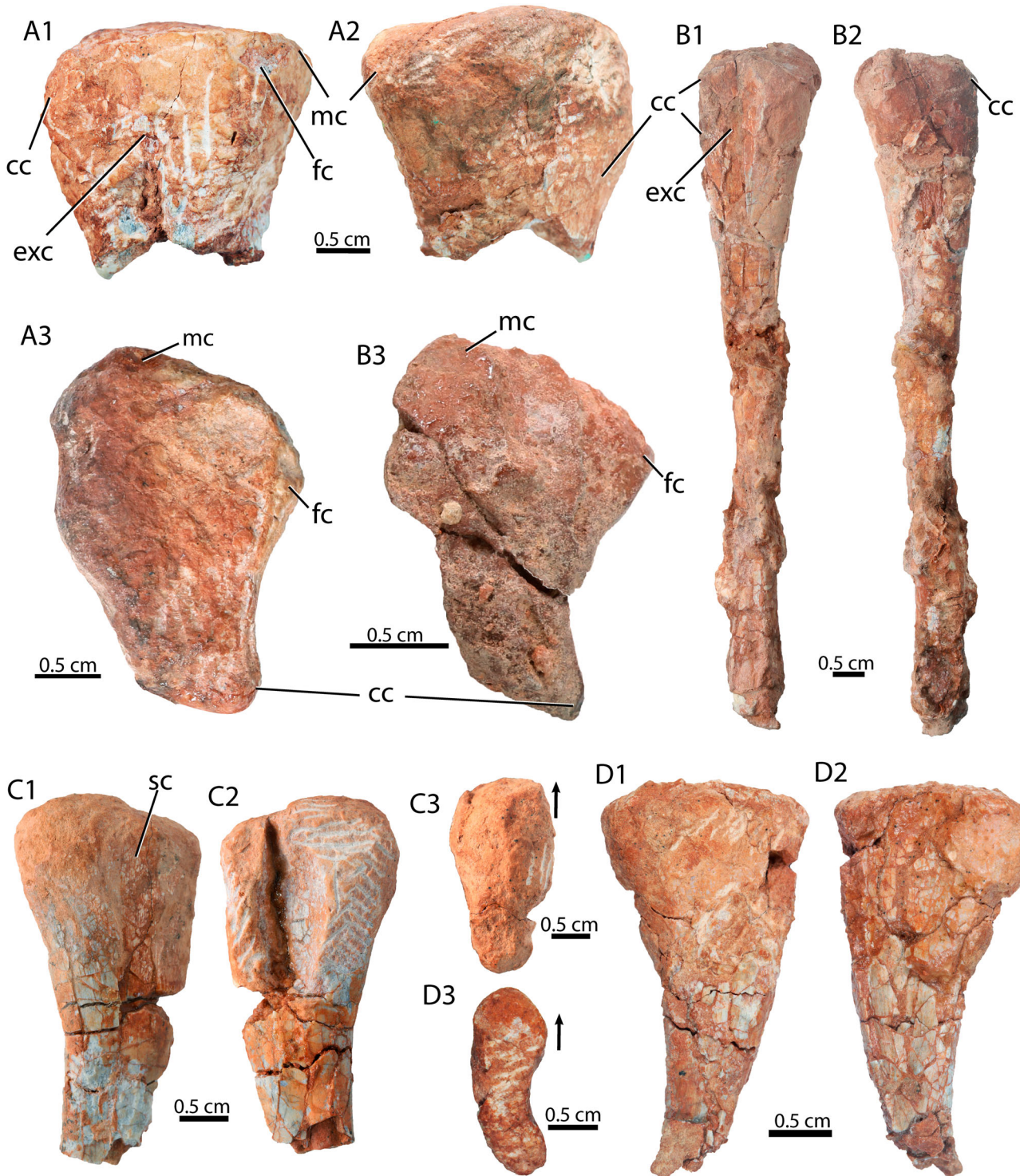


FIGURE 13. UFSM 11579. UFSM 11579R, left tibia: **A1**, lateral view; **A2**, medial view; **A3**, proximal view. UFSM 11579S, left fibula: **B1**, lateral view; **B2**, medial view; **B3**, proximal view. UFSM 11579 T, left fibula: **C1**, lateral view; **C2**, medial view; **C3**, proximal view. UFSM 11579U, left fibula: **D1**, lateral view; **D2**, medial view; **D3**, proximal view. **Abbreviations:** cc, cnemial crest; exc, excavation; fc, fibular condyle; mc, medial condyle; sc, scar. Arrows indicate the anterior direction.

phalanx and has its lateral and medial extremities flanked by constrictions (Fig. 14A, B, D). The distal condyles are laterally, medially, and ventrally expanded compared with the shaft (Fig. 14C, F). A dorsoventral depression is seen in the distal half of the

shaft, separating the well-developed distal condyles. Pits for collateral ligaments are seen at the lateral margin of the distal condyle (Fig. 14A, B). An oval foramen is seen at the center of the lateral surface (Fig. 14B).

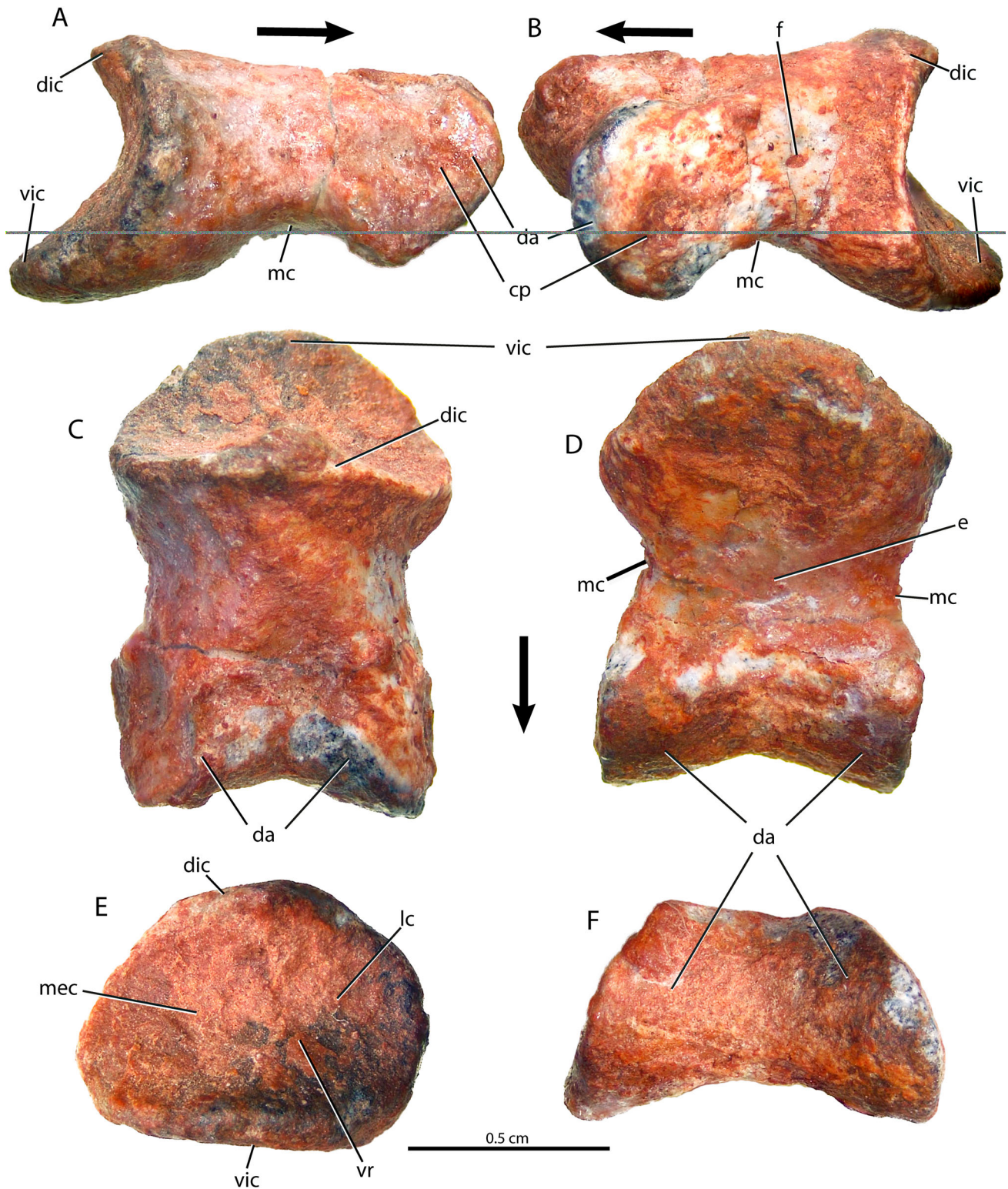


FIGURE 14. UFSM 11579 V, fourth right non-ungual phalanx, possibly from the fourth digit: **A**, lateral view; **B**, medial view; **C**, dorsal view; **D**, ventral view; **E**, proximal view; **F**, distal view. **Abbreviations:** **cp**, collateral pit; **da**, distal articulation; **dic**, dorsal intercondylar process; **e**, excavation; **f**, foramen; **lc**, lateral condyle; **mc**, medial constriction; **mec**, medial condyle; **vic**, ventral intercondylar process; **vr**, ventral ridge.

### Femoral Histology

The left femoral shaft of UFSM115790 was transversely sectioned (Fig. 15), near midshaft. The medullary cavity is filled by calcite crystals. The cortex is densely vascularized (Fig. 15D, E) and the bone tissues exhibit longitudinally oriented primary osteons and occasional anastomoses, a condition typically seen in silesaurids (Fostowicz-Frelik & Sulej, 2010; Griffin & Nesbitt, 2016; Veiga et al., 2018). The microstructure of the cortex is nearly uniform, with no discontinuities such as lines of arrested growth (LAGs—Fig. 15C). It means that UFSM 11579 did not deposit annual LAGs during ontogeny, a feature that may be common for silesaurids (Fostowicz-Frelik & Sulej, 2010; Griffin & Nesbitt, 2016; Veiga et al., 2018). Therefore, UFSM 11579 exhibits a continuous and multi-year growth instead of depositing annual LAGs. As in *Silesaurus opolensis* (Fostowicz-Frelik & Sulej, 2010), *Asilisaurus kongwe* (Griffin & Nesbitt, 2016), *Sacisaurus agudoensis* (Veiga et al., 2018), and *Lewisuchus admixtus* (Ezcurra et al., 2019), UFSM 11579 has no indication of having slowed or stopped its growth before death, differing from the early dinosaur condition, in which LAGs are recorded in the outer cortex of “*Syntarsus*” *rhodesiensis* (Chinsamy, 1990; Chinsamy-Turan, 2008), *Saturnalia tupiniquim* (Stein, 2011), and *Nhandumirim waldsangae* (Marsola et al., 2019a).

The cortex is composed of uninterrupted woven-fibered matrix (i.e., fibrolamellar bone tissue), with more circumferentially oriented fibers at the outermost cortex than at the middle and inner cortices (Fig. 15C). The presence of this type of tissue indicates relatively high rates of bone deposition and, consequently, growth (Amprino, 1947; Francillon-Vieillot et al., 1990; Margerie et al., 2002; Prondvai et al., 2014; Veiga et al., 2018). The entire cortex is well vascularized by primary osteons, which have a longitudinally distributed radial arrangement (Fig. 15C). The tissue shows extensive primary deposition events, as indicated by a thin band of lamellar bone encircling some of the osteons (Fig. 15D, E), which are also surrounded by osteocyte lacunae. As in other dinosauriforms, such as *Asilisaurus kongwe* (Griffin & Nesbitt, 2016), *Lewisuchus admixtus* (Marsà et al., 2017), and *Silesaurus opolensis* (Fostowicz-Frelik & Sulej, 2010), a highly dense array of osteocyte lacunae is present throughout the cortex, with no apparent shape and distribution patterns. Secondary osteons were not observed.

Compared with the osteohistological features of other silesaurid femora, i.e., *Asilisaurus kongwe* (Griffin & Nesbitt, 2016), *Lewisuchus admixtus* (Ezcurra et al., 2019), *Sacisaurus agudoensis* (Veiga et al., 2018), *Silesaurus opolensis* (Fostowicz-Frelik & Sulej, 2010), UFSM 115790 has the same simple vascular arrangement, with longitudinally oriented primary osteons containing few anastomoses, as well as a similar osteocyte

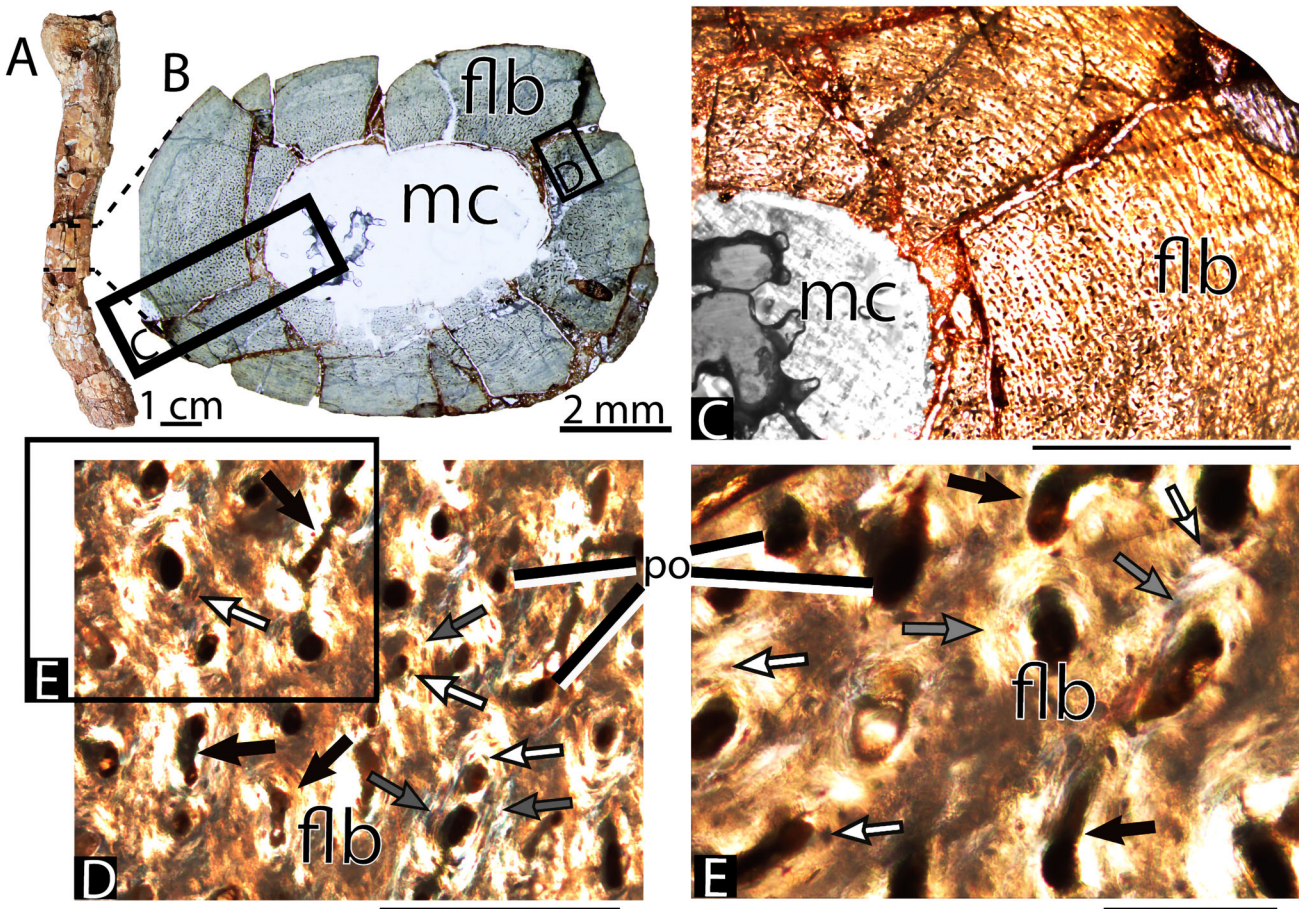


FIGURE 15. Paleohistology of a left femur, UFSM 115790 (Fig. 11E, F), approximately at its mid-length: **A**, lateral view indicating the sampled area of the bone; **B**, cross section of the femur with the square areas detailed in C–E; **C**, view of the complete transect showing the osteohistological pattern of the cortical area showing the pattern of longitudinally oriented primary osteons with few anastomoses; **D**, approximated view of the cortical area showing the pattern of longitudinally oriented primary osteons with few anastomoses; **E**, close-up of an area of D showing details of the primary osteons, anastomoses, and resorption areas. Scale bars from C to E equal 100  $\mu\text{m}$ . **Abbreviations:** flb, fibrolamellar bone; mc, medullary cavity; po, primary osteon; gray arrows, resorption area; white arrows, osteocyte lacunae; black arrows, anastomoses.

lacunae distribution. Yet, UFSM 11579O differs from *Sacisaurus agudoensis* (Veiga et al., 2018) in having fewer anastomoses connecting the longitudinal primary osteons (Fig. 15D, E), resembling more the condition of *Silesaurus opolensis* (Fostowicz-Frelik & Sulej, 2010) and *Lewisuchus admixtus* (Ezcurra et al., 2019). Moreover, the simple vascular arrangement of longitudinally oriented primary osteons of UFSM 11579O and other silesaurids differs from that of most early dinosaurs, the vascular arrangements of which tend to include much more complex anastomoses, i.e., *Massospondylus carinatus* (Klein & Sander, 2007), *Nhandumirim waldsangae* (Marsola et al., 2019a), *Herrerasaurus ischigualastensis* (Padian et al., 2004). In contrast, as pointed out by Veiga et al. (2018), the vascular patterns of Silesauridae seems to approach that of some early ornithischians, such as the *Fruitadens haagarorum* and *Scutello-saurus lawleri* (Butler et al., 2010), which include predominantly longitudinally oriented vascular canals with few anastomoses (Butler et al., 2010; Padian et al., 2004; Veiga et al., 2018). Considering that more complex vascular patterns are associated with higher growth rates (Margerie et al., 2002; Padian & Lamm, 2013; Veiga et al., 2018), the simple vascular pattern of UFSM 11579O implies that, just like other silesaurids, this animal grew relatively slower than most early dinosaurs (Cerda et al., 2014; Klein & Sander, 2007; Marsola et al., 2019a; Padian et al., 2004).

## DISCUSSION

### Assignment to Silesauridae or Closely Related *Silesaurus*-like Taxa

The taxonomic arrangement of Silesauridae as either a monophyletic group outside Dinosauria or a paraphyletic group within Ornithischia is currently under debate. In any case, UFSM 11579 can be generally assigned to Silesauridae by possessing the following typical traits of the clade/grade in combination: marginal leaf-shaped teeth in the dentary and maxilla, delayed ankylosis tooth attachment mode (presence of “ankylotheodonty”), closed ventral margin of the acetabulum, notch ventral to femoral head, femoral head triangular in proximal view, spike-like anterior trochanter in smaller specimens, popliteal fossa extending the distal third of the femur, and a proximodistally elongated dorsolateral trochanter (Ezcurra et al., 2019; Langer & Ferigolo, 2013; Martz & Small, 2019; Mestriner et al., 2022; Nesbitt, 2011; Nesbitt et al., 2019). Additionally, the bone histology of UFSM 11579 exhibits longitudinally oriented primary osteons and occasional anastomoses, a condition typically seen in other silesaurids (Griffin & Nesbitt, 2016; Veiga et al., 2018), and UFSM 11579 did not deposit annual LAGs during ontogeny, a feature that also happens to be common for silesaurids (Fostowicz-Frelik & Sulej, 2010; Griffin & Nesbitt, 2016; Veiga et al., 2018). Although the combination of character states highlighted above clearly validates the UFSM 11579 as a unique silesaurid, regardless of the monophyly or paraphyly of the group, this set of fossils will not be given a new species name. We decided for such a conservative approach mainly because of the incompleteness of the specimen, composed of disarticulated skeletal parts representing several individuals.

### Phylogenetic Analyses and Implications

Scoring UFSM 11579 in the data-matrix of Ezcurra et al. (2019) resulted in 425 most parsimonious trees (MPTs) of 1976 steps, consistency index of 0.267, and retention index of 0.627. As in Ezcurra et al. (2019), the strict consensus of our MPTs shows a large Silesauridae polytomy, here composed by

UFSM 11579 and all other members of the group (*Ignotosaurus fragilis*, *Sacisaurus agudoensis*, *Diodorus scytobrachion*, *Lewisuchus admixtus*, *Eucoelophysis baldwini*, *Lutungutali sitwensis*, *Silesaurus opolensis*, and *Asilisaurus kongwe*—see Supplementary Material, Appendix S1, Fig. S3). Following Ezcurra et al. (2019), we a posteriori pruned *Lutungutali sitwensis*, resulting in 424 most parsimonious trees (MPTs) of 1973 steps, consistency index of 0.268 and retention index of 0.618. In this way, we found a partially resolved Silesauridae, with *Lewisuchus admixtus* as the sister taxon of the other species of the group and *Asilisaurus kongwe* as the sister taxon of all silesaurids except *Lewisuchus admixtus* (Fig. 16A—also see Supplementary Material, Appendix S1, Fig. S1). All silesaurids except for *Lewisuchus admixtus* and *Asilisaurus kongwe* form a polytomy containing UFSM 11579. Branch supports for Silesauridae and for the clade including *Asilisaurus kongwe* and other silesaurids are very low (Bremer support = 1; bootstrap frequencies <20%). Among the synapomorphies recovered here for Silesauridae, UFSM 11579 shares only the presence of “ankylotheodonty” (condition “1” of character 161, scored “0&1” for UFSM 11579). Yet, given the complex nature of this feature (Mestriner et al., 2022), its simple scoring on the characters formulations so far proposed can lead to misleading support. When the previous analysis scores (keeping *Lutungutali sitwensis* pruned) is rerun without character 161, the clade Silesauridae is dismantled, with UFSM 11579, *Ignotosaurus fragilis*, *Sacisaurus agudoensis*, *Diodorus scytobrachion*, *Lewisuchus admixtus*, *Eucoelophysis baldwini*, *Silesaurus opolensis*, and *Asilisaurus kongwe* forming a polytomy outside a monophyletic Dinosauria (Fig. 16B—also see Supplementary Material, Appendix S1, Fig. S2). This analysis resulted in 575 most parsimonious trees (MPTs) of 1971 steps, consistency index of 0.267 and retention index of 0.627. In any case, in the analysis with character 161, UFSM 11579 is found within Silesauridae also because it shares with all members of the group, except *Lewisuchus admixtus*, a femur with a transverse groove on the proximal surface and a popliteal fossa extending proximal to the distal 1/4 of the bone (Fig. 16A). It is worth mentioning that *Nhandumirim waldsangae* scores were added into the data-matrix of Ezcurra et al. (2019) in order to increase the early dinosaurs sampling of this dataset (see Material and methods), and the taxa was recovered within Theropoda (see Supplementary Data, Appendix S1, Fig. S1).

Our analysis including UFSM 11579 in the Müller & Garcia (2020) matrix resulted in 11,321 most parsimonious trees (MPTs) of 989 steps, with a consistency index of 0.316, and a retention index of 0.661. In the strict consensus, UFSM 11579 was found in a huge polytomy outside of the Sauropodomorpha–Theropoda dichotomy (Fig. 16C). We also conducted an exploratory analysis excluding the tooth attachment character 100, which resulted in 3640 most parsimonious trees (MPTs) of 986 steps, with a consistency index of 0.316, and a retention index of 0.662. This partially resolved the topology, with UFSM 11579 found at the base of Ornithischia in another polytomic rearrangement, including most other silesaurids, *Pisanosaurus mertii*, and a clade including all other scored ornithischians (Fig. 16D). *Asilisaurus kongwe*, *Soumyasaurus aenigmaticus*, and *Lewisuchus admixtus*, on the other hand, were recovered in a polytomy with many dinosauriform species and clades (Fig. 16D).

The results of these analyses (Fig. 16) show how unstable the inner relationships of Silesauridae are, in which the addition of one taxon and/or the exclusion of one character is enough to collapse most of the topology. Accordingly, this shows that it is time to investigate new anatomical aspects of the group, paving the way for future studies on their evolutionary relations.

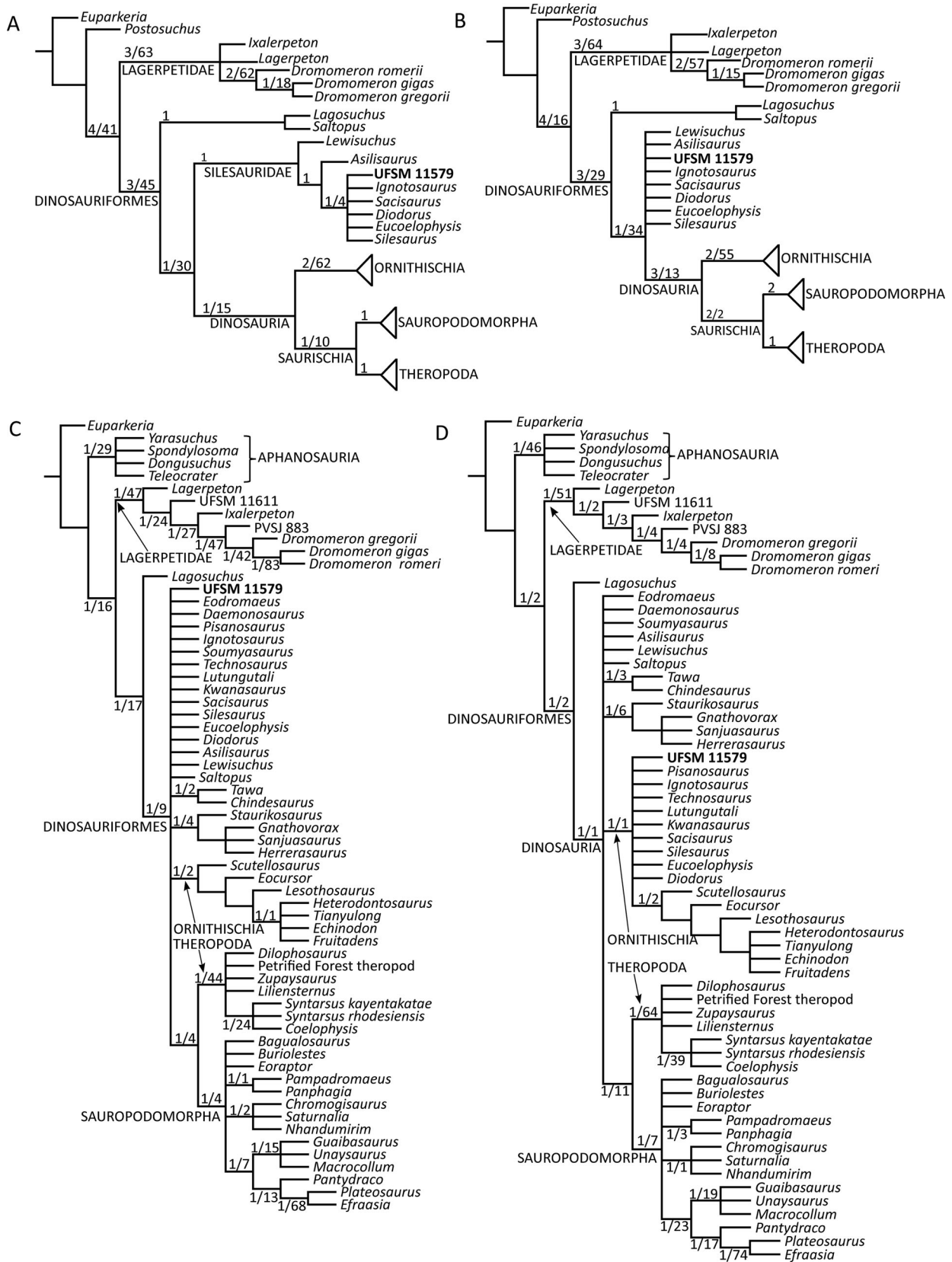


FIGURE 16. Phylogenetic relationships of UFSM 11579 among early dinosauromorphs. **A, B**, UFSM 11579 scored in the Ezcurra et al. (2019) matrix, ornithischians, sauropodomorphs, and theropods were merged into single supraspecific terminals in the figure for the sake of simplicity; **A**, strict reduced consensus tree after a posteriori pruning of *Lutungutali siwensis*; **B**, exploratory analysis (strict reduced consensus tree) excluding the tooth attachment character 161. **C, D**, UFSM 11579 scored in the Müller & Garcia (2020) matrix: **C**, strict consensus tree; **D**, exploratory analysis (strict reduced consensus tree) excluding the tooth attachment character 100. Numbers at the nodes are Bremer support and GC bootstrap frequencies, respectively.

## CONCLUSION

The new discovery represents the second silesaurid record in the Carnian of Brazil, and the first based on a significant amount of skeletal parts. Although still relatively incomplete, UFSM 11579 provides further information concerning the anatomical diversity of Silesauridae. Its postcranium bears a combination of dinosauromorph sympleiomorphies and silesaurid diagnostic features. The phylogenetic analyses reveal labile evolutionary patterns not only for Silesauridae, but for early Dinosauroomorpha in general.

## DATA AVAILABILITY STATEMENT

The raw CT-scan data are available in the following repository: <https://doi.org/10.5281/zenodo.7939011>

## ACKNOWLEDGMENTS

We thank researchers, collection managers, and curators who provided access to the collections under their care, namely: A. Downs, A.M. Ribeiro, A. Silveira, C. Apaldetti, C. Schultz, C. Revuelta, F. Abdala, F. Novas, F. Pretto, G. Cisterna, G. Gurtler, J. Ferigolo, L. Haerter, L. Kerber, M. Ezcurra, M. Caldwell, M. Stocker, P. Ortíz, P. Hernández, R. Müller, R. Martínez, and S. Cabreira. Thanks also to V. Yarborough, Paleontology Laboratory Manager at Virginia Tech, who accurately improved the preparation of the fossils, and to R. Piechowski, University of Warsaw, for giving permission to use one photo of the *Silesaurus opolensis* maxilla. Thanks to D. Casali for his help, tips, and suggestions with Mesquite and TNT software. The authors also acknowledge the support provided by Centro para Documentação da Biodiversidade, FFCLRP, Universidade de São Paulo, Brazil, regarding the use of the CT-scan (computed tomography) machine. Thanks to the JVP editors M. D'Emic (Senior Editor), D. Schwartz (Editor, Journal of Vertebrate Paleontology), P. Godoy (Phylogenetics Editor, Journal of Vertebrate Paleontology), and two anonymous reviewers. Finally, the authors acknowledge the São Paulo Research Foundation (FAPESP), Coordination for the Improvement of Higher Education Personnel (CAPES), National Council for Technologic and Scientific Research (CNPq), and the National Science Foundation (NSF) EAR for funding this research.

The São Paulo Research Foundation awarded grants to Gabriel Mestriner (FAPESP 2022/00171-9, 2019/07510-0, and 2018/24031-6), to Júlio Marsola (FAPESP 2021/14560-4), and to Max Langer (FAPESP 2020/07997-4). Coordination for the Improvement of Higher Education Personnel supported Júlio Marsola (CAPES 88887.572782/2020-00). The National Council for Technologic and Scientific Development supported Átila Da-Rosa (CNPq 303972/2021-1). The National Science Foundation supported Sterling Nesbitt (NSF 1349667).

## AUTHOR CONTRIBUTIONS

JCAM and AASDR played significant roles in the discovery and excavation of the fossil during a joint fieldwork expedition in 2014, which was conducted by the Laboratório de Paleontologia (Universidade de São Paulo—USP, Ribeirão Preto) and the Laboratório de Estratigrafia e Paleobiologia (Universidade Federal de Santa Maria—UFSM, Santa Maria). GM, JCAM, and ML designed the project. GM and SJN performed the mechanical preparation of the fossils. GM conducted the anatomical descriptions, created the figures, and drafted the manuscript. GM and JCAM carried out the phylogenetic analysis. AASDR contributed valuable geological information. All authors actively participated in editing the manuscript and engaging in fruitful

discussions regarding the data, results, and implications of the new silesaurid specimen.

## LIST OF SUPPLEMENTARY FILES

## SUPPLEMENTAL DATA (APPENDICES S1 AND S2).

Matrix of Ezcurra et al., 2019: TNT and NEXUS files. Plus, MPTs of the parsimony analyses: 1, MPTs—Ezcurra et al., 2019—analysis corresponding to Fig. 3 of the supplementary material; 2, MPTs—Ezcurra et al., 2019—analysis corresponding to Fig. 16A of the Main Document; 3, MPTs—Ezcurra et al., 2019—analysis corresponding to Fig. 16B of the Main Document TNT file: Ezcurra et al., 2020.

Matrix of Muller & Garcia 2020: TNT and NEXUS files. Plus, MPTs of the parsimony analyses: 1, MPTs—Muller & Garcia 2020—Analysis corresponding to Fig. 16C; 2, MPTs—Muller & Garcia 2020—Analysis corresponding to Fig. 16D.

Raw images of the histology (Fig. 15): 1, Raw data—histology—Corresponding to Fig. 15C; 2, Raw data—Histology—Corresponding to Fig. 15D; 3, Raw data—Histology—Corresponding to the Fig. 15E.

## ORCID

Gabriel Mestriner  <http://orcid.org/0000-0002-5542-1772>

Júlio C. A. Marsola  <http://orcid.org/0000-0001-5290-7884>

Sterling J. Nesbitt  <http://orcid.org/0000-0002-7017-1652>

Átila Augusto Stock Da-Rosa  <http://orcid.org/0000-0003-4074-0794>

Max Langer  <http://orcid.org/0000-0003-1009-4605>

## LITERATURE CITED

- Agnolin, F.L. & Ezcurra, M.D. (2019). The validity of *Lagosuchus talampayensis* Romer, 1971 (Archosauria, Dinosauriformes), from the Late Triassic of Argentina. *Breviora*, 565(1), 1–21. <https://doi.org/10.3099/0006-9698-565.1.1>.
- Agnolin, F.L., & Rozadilla, S. (2018). Phylogenetic reassessment of *Pisanosaurus mertii* Casamiquela, 1967, a basal dinosauriform from the Late Triassic of Argentina. *Journal of Systematic Palaeontology*, 16(10), 853–879. <https://doi.org/10.1080/14772019.2017.1352623>.
- Amprino, R. (1947). La structure du tissu osseux envisagée comme expression de différences dans la vitesse de l'accroissement. *Archives de biologie*, 58(4), 317–330.
- Andreis, R., Bossi, G.E., & Montardo, D.K. (1980). O Grupo Rosário do Sul (Triássico) no Rio Grande do Sul. 659–673. In *Anais do XXXI Congresso Brasileiro de Geologia, Camboriú, Santa Catarina. Sociedade Brasileira de Geologia, Sao Paulo, Brazil*.
- Baron, M., Norman, D. B. & Barrett, P. (2017a). A new hypothesis of dinosaur relationships and early dinosaur evolution. *Nature* 543, 501–506. <https://doi.org/10.1038/nature21700>.
- Baron, M. G., Norman, D. B., & Barrett, P. M. (2017b). Postcranial anatomy of *Lesothosaurus diagnosticus* (Dinosauria: Ornithischia) from the Lower Jurassic of southern Africa: implications for basal ornithischian taxonomy and systematics. *Zoological Journal of the Linnean Society*, 179(1), 125–168. <https://doi.org/10.1111/zoj.12434>.
- Benton, M. J., Forth J., & Langer, M. C. (2014). Models for the rise of the dinosaurs. *Current Biology*, 24(2), R87–R95. <https://doi.org/10.1016/j.cub.2013.11.063>.
- Benton, M.J., & Walker, A. D. (2011). *Saltopus*, a dinosauriform from the Upper Triassic of Scotland. *Earth and Environmental Science Transactions of the Royal Society of Edinburgh*, 101(3–4), 285–299. <https://doi.org/10.1017/S1755691011020081>.
- Bittencourt, J. D. S., Arcucci A. B., Marsicano C. A., & Langer, M. C. (2015). Osteology of the Middle Triassic archosaur *Lewisuchus admixtus* Romer (Chañares Formation, Argentina), its inclusivity, and relationships amongst early dinosauromorphs. *Journal of Systematic Palaeontology*, 13(3), 189–219. <https://doi.org/10.1080/14772019.2013.878758>.



- Bittencourt, J. D. S., & Kellner, A. W. A. (2009). The anatomy and phylogenetic position of the Triassic dinosaur *Staurikosaurus pricei* Colbert, 1970. *Zootaxa*, 2079(1), 1–56. <https://doi.org/10.11646/zootaxa.2079.1.1>.
- Brusatte, S. L., Benton, M. J., Ruta, M., & Lloyd, G. T. (2008). Superiority, competition, and opportunism in the evolutionary radiation of dinosaurs. *Science*, 321(5895), 1485–1488. <https://doi.org/10.1126/science.1161833>.
- Brusatte, S. L., Nesbitt, S. J., Irmis, R. B., Butler, R. J., Benton, M. J., & Norell, M. A. (2010). The origin and early radiation of dinosaurs. *Earth-Science Reviews*, 101(1–2), 68–100. <https://doi.org/10.1016/j.earscirev.2010.04.001>.
- Butler, R. J. (2010). The anatomy of the basal ornithischian dinosaur *Eocursor parvus* from the lower Elliot Formation (Late Triassic) of South Africa. *Zoological Journal of the Linnean Society*, 160(4), 648–684. <https://doi.org/10.1111/j.1096-3642.2009.00631.x>.
- Butler, R. J., Galton, P. M., Porro, L. B., Chiappe, L. M., Henderson, D. M., & Erickson, G. M. (2010). Lower limits of ornithischian dinosaur body size inferred from a new Upper Jurassic heterodontosaurid from North America. *Proceedings of the Royal Society B: Biological Sciences*, 277(1680), 375–381. <https://doi.org/10.1098/rspb.2009.1494>.
- Butler, R. J., Porro, L. B., & Norman, D. B. (2008). A juvenile skull of the primitive ornithischian dinosaur *Heterodontosaurus tucki* from the ‘Stormberg’ of southern Africa. *Journal of Vertebrate Paleontology*, 28, 702–711. <https://doi.org/10.1671/0272>.
- Cabreira, S. F., Kellner, A. W. A., Dias-da-Silva, S., da Silva, L. R., Bronzati, M., Marsola, J. C., Müller, R. T., Bittencourt, J. S., Batista, B. J., Raugust, T., Carrilho, R., Brodt, A., & Langer, M. C. (2016). A unique Late Triassic dinosauriform assemblage reveals dinosaur ancestral anatomy and diet. *Current Biology*, 26(22), 3090–3095. <https://doi.org/10.1016/j.cub.2016.09.040>.
- Casamiquela, R. M. (1967). Un nuevo dinosaurio ornithischio triásico (*Pisanosaurus mertii*; Ornithopoda) de la Formación Ischigualasto, Argentina. *Ameghiniana*, 5(2), 47–64.
- Cerda, I. A., Pol, D., & Chinsamy, A. (2014). Osteohistological insight into the early stages of growth in *Mussaurus patagonicus* (Dinosauria, Sauropodomorpha). *Historical Biology*, 26(1), 110–121. <https://doi.org/10.1080/08912963.2012.763119>.
- Chatterjee, S. (1984). A new ornithischian dinosaur from the Triassic of North America. *Naturwissenschaften*, 71(12), 630–631. DOI:10.1007/BF00377897.
- Chinsamy-Turan, A. (1990). Physiological implications of the bone histology of *Syntarsus rhodesiensis* (Saurischia: Theropoda). *Palaeontologia africana*, 27, 77–82.
- Chinsamy-Turan, A. (2008). The microstructure of dinosaur bone: deciphering biology with fine-scale techniques. *Zoological Journal*, 154(3), 631–632. <https://doi.org/10.1111/j.1096-3642.2008.00476.x>.
- Coddington, J. A., & Scharff, N. (1994). Problems with zero-length branches. *Cladistic* 10, 415–423.
- Da Rosa, Á. A. S. (2004). Sítios fossilíferos de Santa Maria, RS. *Ciência & Natura* 26, 5–90.
- Da Rosa, Á. A. S. (2005). Palealterações em depósitos sedimentares deplancias aluviais do Triássico Médio a Superior do sul do Brasil: caracterização, análise estratigráfica e preservação fossilífera. *UNISINOS, São Leopoldo*. 2005.
- Da Rosa, Á. A. S. (2015). Geological context of the dinosauriform-bearing outcrops from the Triassic of Southern Brazil. *Journal of South American Earth Sciences* 61, 108–119. <https://doi.org/10.1016/j.jsames.2014.10.008>.
- Desojo, J. B., Fiorelli, L. E., Ezcurra, M. D., Martinelli, A. G., Ramezani, J., Da Rosa, Á. A., von Baczko, M. B., Trotteyn, M. J., Montefeltro, F. C., Ezpeleta, M., & Langer, M. C. (2020). The Late Triassic Ischigualasto Formation at Cerro Las Lajas (La Rioja, Argentina): fossil tetrapods, high-resolution chronostratigraphy, and faunal correlations. *Scientific Reports*, 10(1), 1–34. <https://doi.org/10.1038/s41598-020-67854-1>.
- Dzik, J. (2003). A beaked herbivorous archosaur with dinosaur affinities from the early Late Triassic of Poland. *Journal of Vertebrate Paleontology* 23(3), 556–574. <https://doi.org/10.1671/A1097>.
- Eltink, E., Da-Rosa, Á. A. S., & Dias-da-Silva, S. (2017). A capitosauroid from the Lower Triassic of South America (Sanga do Cabral Supersequence: Paraná Basin), its phylogenetic relationships and biostratigraphic implications. *Historical Biology*, 29(7), 863–874. <https://doi.org/10.1080/08912963.2016.1255736>.
- Ezcurra, M. D. (2006). A review of the systematic position of the dinosauriform archosaur *Eucoelophysis baldwini* Sullivan & Lucas, 1999 from the Upper Triassic of New Mexico, USA. *Geodiversitas*, 28(4), 649–684.
- Ezcurra, M. D., Nesbitt, S. J., Fiorelli, L. E., & Desojo, J. B. (2019). New specimen sheds light on the anatomy and taxonomy of the early Late Triassic dinosauriforms from the Chañares Formation, NW Argentina. *The Anatomical Record*, 303(5), 1393–1438. <https://doi.org/10.1002/ar.24243>.
- Ferigolo, J., & Langer, M. C. (2007). A Late Triassic dinosauriform from south Brazil and the origin of the ornithischian predecestry bone. *Historical Biology*, 19(1), 23–33. <https://doi.org/10.1080/08912960600845767>.
- Fostowicz-Frelik, Ł., & Sulej, T. (2010). Bone histology of *Silesaurus opolensis* Dzik, 2003 from the Late Triassic of Poland. *Lethaia*, 43(2), 137–148. <https://doi.org/10.1111/j.1502-3931.2009.00179.x>.
- Francillon-Vieillot, H., Buffrénil, V., Castanet, J., Géraudie, J., Meunier, F. J., Sire, J. Y., Zylberberg, L., & Ricqlès, A. (1990). Microstructure and mineralization of vertebrate skeletal tissues. *Skeletal biominer-alization: patterns, processes and evolutionary trends*, 1, 471–530.
- Gauthier, J. (1986). Saurischian monophyly and the origin of birds. *Memoirs of the California Academy of sciences*, 8, 1–55. <https://doi.org/10.1017/S24752630000091X>.
- Goloboff, P. A., & Catalano, S. A. (2016). TNT version 1.5, including a full implementation of phylogenetic morphometrics. *Cladistics*, 32(3), 221–238. <https://doi.org/10.1111/cla.12160>.
- Goloboff, P. A., Farris, J. S., Källersjö, M., Oxelman, B., Ramírez, M. J., & Szumik, C. A. (2003). Improvements to resampling measures of group support. *Cladistics*, 19(4), 324–32. <https://doi.org/10.1111/j.1096-0031.2003.tb00376.x>.
- Goloboff, P. A., Farris, J. S., & Nixon, K. C. (2008). TNT, a free program for phylogenetic analysis. *Cladistics*, 24(5), 774–786. <https://doi.org/10.1111/j.1096-0031.2008.00217.x>.
- Gordon, M. (1947). Classificação das formações gondwânicas do Paraná, Santa Catarina e Rio Grande do Sul. *Notas Preliminares e Estudos, DNPM/DGM, Rio de Janeiro* 38, 1–20.
- Griffin, C. T., & Nesbitt, S. J. (2016). The femoral ontogeny and long bone histology of the Middle Triassic (? late Anisian) dinosauriform *Asilisaurus kongwe* and implications for the growth of early dinosaurs. *Journal of Vertebrate Paleontology*, 36(3), e1111224. <https://doi.org/10.1080/02724634.2016.1111224>.
- Hendrickx, C., Mateus, O., & Araújo, R. (2015). A proposed terminology of theropod teeth (Dinosauria, Saurischia). *Journal of Vertebrate Paleontology*, 35(5), e982797. <https://doi.org/10.1080/02724634.2015.982797>.
- Horn, B. L. D., Melo, T. M., Schultz, C. L., Philipp, R. P., Kloss, H. P., & Goldberg, K. (2014). A new third-order sequence stratigraphic framework applied to the Triassic of the Paraná Basin, Rio Grande do Sul, Brazil, based on structural, stratigraphic and paleontological data. *Journal of South American Earth Sciences*, 55, 123–132. <https://doi.org/10.1016/j.jsames.2014.07.007>.
- Huene, F. V. (1942). Die fossilen Reptilien des Südamerikanischen Südwandalandes. Ergebnisse der Sauriergrabungen in Südbrasilien, 1928/1929. *C. H. Beck'sche Verlagsbuchhandlung, Munich*, 161–332.
- Huene, F. V. (1928). Ein Cynodontier aus der Trias Brasiliens. *Centralblatt für Mineralogie, Geologie und Paläontologie* B, 251–270.
- Irmis, R. B., Nesbitt, S. J., Padian, K., Smith, N. D., Turner, A. H., Woody, D., & Downs, A. (2007). A late Triassic Dinosauriform assemblage from New Mexico and the rise of dinosaurs. *Science*, 317(5836), 358–361. DOI: 10.1126/science.1143325.
- Kammerer, C. F., Nesbitt, S. J., & Shubin, N. H. (2011). The first silesaurid dinosauriform from the Late Triassic of Morocco. *Acta Palaeontologica Polonica*, 57(2), 277–284. <https://doi.org/10.4202/app.2011.0015>.
- Klein, N., & Sander, P. M. (2007). Bone histology and growth of the pro-sauropod *Plateosaurus engelhardti* Meyer, 1837 from the Norian bonebeds of Trossingen (Germany) and Frick (Switzerland). *Special Papers in Palaeontology* 77, 169–206.
- Langer, M. C. (2003). The pelvic and hind limb anatomy of the stem sauropodomorph *Saturnalia tupiniquim* (Late Triassic, Brazil). *PaleoBios*, 23, 1–40.
- Langer, M. C. (2005a). Studies on continental Late Triassic tetrapod biochronology. I. The type locality of *Saturnalia tupiniquim* and the faunal succession in south Brazil. *Journal of South American*

- Earth Sciences*, 19:205–218. <https://doi.org/10.1016/j.jsames.2005.04.003>.
- Langer, M. C. (2005b). Studies on continental Late Triassic tetrapod biochronology. II. The Ischigualastian and a Carnian global correlation. *Journal of South American Earth Sciences*, 19, 219–239. <https://doi.org/10.1016/j.jsames.2005.04.002>.
- Langer, M. C. (2014). The origins of Dinosauria: much ado about nothing. *Palaeontology*, 57(3), 469–478. <https://doi.org/10.1111/pala.12108>.
- Langer, M. C., Abdala, F., Richter, M., & Benton, M. J. (1999). A sauropodomorph dinosaur from the Upper Triassic (Carnian) of southern Brazil. *Comptes Rendus de l'Academie des Sciences*, 329, 511–517. [https://doi.org/10.1016/S1251-8050\(00\)80025-7](https://doi.org/10.1016/S1251-8050(00)80025-7).
- Langer, M. C., & Benton, M. J. (2006). Early dinosaurs: a phylogenetic study. *Journal of Systematic Palaeontology*, 4(4), 309–358. <https://doi.org/10.1017/S1477201906001970>.
- Langer, M. C., Ezcurra, M. D., Bittencourt, J. S., & Novas, F. E. (2010). The origin and early evolution of dinosaurs. *Biological Reviews*, 85(1), 55–110. <https://doi.org/10.1111/j.1469-185X.2009.00094.x>.
- Langer, M. C., Ezcurra, M. D., Rauhut, O. W., Benton, M. J., Knoll, F., McPhee, B. W., Novas, F. E., Pol, D., & Brusatte, S. L. (2017). Untangling the dinosaur family tree. *Nature*, 551(7678), E1–E3. <https://doi.org/10.1038/nature21700>.
- Langer, M. C., & Ferigolo, J. (2013). The Late Triassic dinosauriform *Sacisaurus agudoensis* (Caturrita Formation; Rio Grande do Sul, Brazil): anatomy and affinities. *Geological Society, London, Special Publications*, 379(1), 353–392. <https://doi.org/10.1144/SP379.16>.
- Langer, M. C., Nesbitt, S. J., Bittencourt, J. S., & Irmis, R. B. (2013). Non-dinosaurian dinosauriforms. *Geological Society, London, Special Publications*, 379(1), 157–186. <https://doi.org/10.1144/SP379.9>.
- Langer, M. C., Ramezani, J., & Da Rosa, A. S. (2018). U-Pb age constraints on dinosaur rise from South Brazil. *Gondwana Research*, 57, 133–140. <https://doi.org/10.1016/j.gr.2018.01.005>.
- Langer, M. C., Ribeiro, A. M., Schultz, C. L., & Ferigolo, J. (2007). The continental tetrapod-bearing Triassic of South Brazil. *New Mexico Museum of Natural History and Science Bulletin*, 41, 201–218.
- LeBlanc, A. R. H., Brink, K. S., Cullen, T. M., & Reisz, R. R. (2017). Evolutionary implications of tooth attachment versus tooth implantation: a case study using dinosaur, crocodylian, and mammal teeth. *Journal of Vertebrate Paleontology*, 37(5), e1354006. <https://doi.org/10.1080/02724634.2017.1354006>.
- Luca, S., & Luca, A. P. (1980). The postcranial skeleton of *Heterodontosaurus tucki* (Reptilia, Ornithischia) from the Stormberg of South Africa. *Annals of the South African Museum*, 79, 159–211.
- Margerie, E., Cubo, J., & Castanet, J. (2002). Bone typology and growth rate: testing and quantifying 'Amprino's rule' in the mallard (*Anas platyrhynchos*). *Comptes rendus biologies*, 325(3), 221–230. [https://doi.org/10.1016/S1631-0691\(02\)01429-4](https://doi.org/10.1016/S1631-0691(02)01429-4).
- Marsà, J. A. G., Agnolín, F. L., & Novas, F. (2017). Bone microstructure of *Lewisuchus admixtus* Romer, 1972 (Archosauria, Dinosauriformes). *Historical Biology*, 31(2), 157–162. <https://doi.org/10.1080/08912963.2017.1347646>.
- Marsola, J. C., Bittencourt, J. S., Butler, R. J., Da Rosa, A. A., Sayão, J. M., & Langer, M. C. (2019a). A new dinosaur with theropod affinities from the Late Triassic Santa Maria Formation, South Brazil. *Journal of Vertebrate Paleontology*, 38(5), e1531878. <https://doi.org/10.1080/02724634.2018.1531878>.
- Marsola, J. C., Bittencourt, J. S., Da Rosa, A. A., Martinelli, A. G., Ribeiro, A. M., Ferigolo, J., & Langer, M. C. (2018). New sauropodomorph and cynodont remains from the late Triassic *Sacisaurus* site in Southern Brazil and its stratigraphic position in the Norian Caturrita Formation. *Acta Palaeontologica Polonica*, 63(4), 653–669. <https://doi.org/10.4202/app.00492.2018>.
- Marsola, J. C., Ferreira, G. S., Langer, M. C., Button, D. J., & Butler, R. J. (2019b). Increases in sampling support the southern Gondwanan hypothesis for the origin of dinosaurs. *Palaeontology*, 62(3), 473–482. <https://doi.org/10.5061/dryad.6t5m946>.
- Martinelli, A. G., Eltink, E., Da Rosa, A. A., & Langer, M. C. (2017). A new cynodont from the Santa Maria Formation, south Brazil, improves Late Triassic probainognathian diversity. *Papers in Palaeontology* 3, 401–423. <https://doi.org/10.5061/dryad.q2m2v>.
- Martínez, R. N., Apaldetti, C., Alcober, O. A., Colombi, C. E., Sereno, P. C., Fernandez, E., Malnis, P. S., Correa, G. A. & Abelin, D. (2012). Vertebrate succession in the Ischigualasto Formation. *Journal of Vertebrate Paleontology*, 32, 10–30. <https://doi.org/10.1080/02724634.2013.818546>.
- Martínez, R. N., Sereno, P. C., Alcober, O. A., Colombi, C. E., Renne, P. R., Montañez, I. P., & Currie, B. S. (2011). A basal dinosaur from the dawn of the dinosaur era in southwestern Pangaea. *Science*, 331(6014), 206–210. <https://doi.org/10.1126/science.119846>.
- Martz, J. W., & Small, B. J. (2019). Non-dinosaurian dinosauriforms from the Chinle Formation (Upper Triassic) of the Eagle Basin, northern Colorado: *Dromomeron romeri* (Lagerpetidae) and a new taxon, *Kwanasaurus williamparkeri* (Silesauridae). *PeerJ*, 7, e7551. <https://doi.org/10.7717/peerj.7551>.
- Mestriner, G., LeBlanc, A. R. H., Nesbitt, S. J., Marsola, J. C. A., Irmis, R. B., Da Rosa, A. A., Ribeiro, A. M., Ferigolo, J., & Langer, M. C. (2022). Histological analysis of ankylothercodonty in Silesauridae (Archosauria: Dinosauriformes) and its implications for the evolution of dinosaur tooth attachment. *The Anatomical Record*, 305(2), 393–423. <https://doi.org/10.1002/ar.24679>.
- Müller, R. T., & Garcia, M. S. (2023). A new silesaurid from Carnian beds of Brazil fills a gap in the radiation of avian line archosaurs. *Scientific Reports*, 13(1), 4981. <https://doi.org/10.1038/s41598-023-32057-x>.
- Müller, R. T., & Garcia, M. S. (2020). A paraphyletic 'Silesauridae' as an alternative hypothesis for the initial radiation of ornithischian dinosaurs. *Biology Letters*, 16(8), 20200417. <https://doi.org/10.1098/rsbl.2020.0417>.
- Nesbitt, S. J. (2011). The early evolution of archosaurs: relationships and the origin of major clades. *Bulletin of the American Museum of Natural History*, 352(1), 1–292. <http://doi.org/10.1206/352.1>.
- Nesbitt, S. J., Butler, R. J., Ezcurra, M. D., Barrett, P. M., Stocker, M. R., Angielczyk, K. D., Smith, R. M. H., Sidor, C. A., Niedzwiedzki, G., Sennikov, A. G., & Charig, A. J. (2017a). The earliest bird-line archosaurs and the assembly of the dinosaur body plan. *Nature*, 544(7651), 484–487. <https://doi.org/10.1038/nature22037>.
- Nesbitt, S. J., Butler, R. J., Ezcurra, M. D., Charig, A. J., & Barrett P. M. (2017b). The anatomy of *Teleocrater rhadinus*, an early avemetatarsalian from the lower portion of the Lufua Member of the Manda Beds (Middle Triassic). *Journal of Vertebrate Paleontology*, 37, 142–177. <https://doi.org/10.1080/02724634.2017.1396539>.
- Nesbitt, S. J., Irmis, R. B., & Parker, W. G. (2007). A critical re-evaluation of the Late Triassic dinosaur taxa of North America. *Journal of Systematic Palaeontology*, 5(2), 209–243. <https://doi.org/10.1017/S1477201907002040>.
- Nesbitt, S. J., Irmis, R. B., Parker, W. G., Smith, N. D., Turner, A. H., & Rowe, T. (2009). Hindlimb osteology and distribution of basal dinosauriforms from the Late Triassic of North America. *Journal of Vertebrate Paleontology*, 29(2), 498–516. <https://doi.org/10.1671/039.029.0218>.
- Nesbitt, S. J., Langer, M. C., & Ezcurra, M. D. (2019). The anatomy of *Asilisaurus kongwe*, a dinosauriform from the Lufua Member of the Manda Beds (~ Middle Triassic) of Africa. *The Anatomical Record*, 303(4), 813–873. <https://doi.org/10.1002/ar.24287>.
- Nesbitt, S. J., Sidor, C. A., Irmis, R. B., Angielczyk, K. D., Smith, R. M., & Tsuji, L. A. (2010). Ecologically distinct dinosaurian sister group shows early diversification of Ornithodira. *Nature*, 464(7285), 95. <https://doi.org/10.1038/nature08718>.
- Norman, D. B., Baron, M. G., Garcia, M. S., & Müller, R. T. (2022). Taxonomic, palaeobiological and evolutionary implications of a phylogenetic hypothesis for Ornithischia (Archosauria: Dinosauria). *Zoological Journal of the Linnean Society*, 196(4), 1273–1309. <https://doi.org/10.1093/zoolinnean/zlac062>.
- Novas, F. E., Agnolín, F. L., Ezcurra, M. D., Müller, R. T., Martinelli, A., & Langer, M. C. (2021). Review of the fossil record of early dinosaurs from South America, and its phylogenetic implications. *Journal of South American Earth Sciences*, 110, 103341. <https://doi.org/10.1016/j.jsames.2021.103341>.
- Novas, F. E. (1996). Dinosaur monophyly. *Journal of Vertebrate Paleontology*, 16(4), 723–741. <https://doi.org/10.1080/02724634.1996.10011361>.
- Novas, F. E., 1992. La evolución de los dinosaurios carnívoros. In Los dinosaurios y su entorno biótico: II Curso de Paleontología, 10 a 12 de julio de 1990. *Actas*, 125–163.
- Novas, F. E. (1994). New information on the systematics and postcranial skeleton of *Herrerasaurus ischigualastensis* (Theropoda: Herrerasauridae) from the Ischigualasto Formation (Upper

- Triassic) of Argentina. *Journal of Vertebrate Paleontology*, 13(4), 400–423. <https://doi.org/10.1080/02724634.1994.10011523>.
- Padian, K., Horner, J. R., & Ricqlès, A. (2004). Growth in small dinosaurs and pterosaurs: the evolution of archosaurian growth strategies. *Journal of Vertebrate Paleontology*, 24(3), 555–571. <https://doi.org/10.1671/0272-4634>.
- Padian, K., & Lamm, E.T. (2013). *Bone histology of fossil tetrapods: advancing methods, analysis, and interpretation*. University of California Press.
- Peacock, B. R., Sidor, C. A., Nesbitt, S. J., Smith, R. M., Steyer, J. S., & Angielczyk, K. D. (2013). A new silesaurid from the upper Ntawere Formation of Zambia (Middle Triassic) demonstrates the rapid diversification of Silesauridae (Avemetatarsalia, Dinosauriformes). *Journal of Vertebrate Paleontology*, 33(5), 1127–1137. <https://doi.org/10.1080/02724634.2013.755991>.
- Pretto, F. A., Müller, R. T., Moro, D., Garcia, M. S., Neto, V. D. P. & Da Rosa, Á. A. S., (2022). The oldest South American silesaurid: New remains from the Middle Triassic (Pinheiros-Chiniquá Sequence, Dinodontosaurus Assemblage Zone) increase the time range of silesaurid fossil record in southern Brazil. *Journal of South American Earth Sciences*, 120, 104039. <https://doi.org/10.1016/j.jsames.2022.104039>.
- Prondvai, E., Stein, K. H., De Ricqlès, A., & Cubo, J. (2014). Development-based revision of bone tissue classification: the importance of semantics for science. *Biological Journal of the Linnean Society*, 112(4), 799–816. <https://doi.org/10.1111/bij.12323>.
- Qvarnström, M., Wernström, J. V., Piechowski, R., Talanda, M., Ahlberg, P. E., & Niedzwiedzki, G. (2019). Beetle-bearing coprolites possibly reveal the diet of a Late Triassic dinosauriform. *Royal Society Open Science*, 6(3), 181042. <https://doi.org/10.1098/rsos.181042>.
- Rauhut, O. W. M. (2003). The interrelationships and evolution of basal theropod dinosaurs. *Special Papers in Palaeontology*, 69, 1–213. <https://doi.org/10.1017/S0016756803248834>.
- Romer, A. S. (1972). The Chañares (Argentina) Triassic reptile fauna. XIV. *Lewisuchus admixtus* a further thecodont from the Chamares Bed. *Breviora* 390, 1–13.
- Sarigul, V., Agnolin, F., & Chatterjee, S. (2018). Description of a multi-taxic bone assemblage from the Upper Triassic Post Quarry of Texas (Dockum Group), including a new small basal dinosauriform taxon. *Historia Natural, Tercera Serie Volumen 8* (1), 5–24.
- Schultz, C. L., Martinelli, A. G., Soares, M. B., Pinheiro, F. L., Kerber, L., Horn, B. L., Preto, F. A., Müller, R. T., & Melo, T. P. (2020). Triassic faunal successions of the Paraná Basin, southern Brazil. *Journal of South American Earth Sciences*, 104, 102846. <https://doi.org/10.1016/j.jsames.2020.102846>.
- Sereno, P. C., & Arcucci, A. B. (1994). Dinosaurian precursors from the Middle Triassic of Argentina: *Marasuchus lilloensis*, gen. nov. *Journal of Vertebrate Paleontology*, 14(1), 53–73. <https://doi.org/10.1080/02724634.1994.10011538>
- Stein, K. H. W. (2011). *Long bone histology of basalmost and derived Sauropodomorpha: the convergence of fibrolamellar bone and the evolution of gigantism and nanism*. [Unpublished doctoral's dissertation]. Universitäts- und Landesbibliothek Bonn.
- Sullivan, R. M., & Lucas, S. G. (1999). *Eucoelophysis baldwini* a new theropod dinosaur from the Upper Triassic of New Mexico, and the status of the original types of Coelophysis. *Journal of Vertebrate Paleontology*, 19(1), 81–90. <https://doi.org/10.1080/02724634.1999.10011124>.
- Tykoski, R. (2005). *Osteology, ontogeny, and relationships of the coelophysoid theropods*. [Unpublished doctoral's dissertation]; The University of Texas, Austin.
- Veiga, F. H., Botha-Brink, J., Ribeiro, A. ., Ferigolo, J., & Soares, M.B. (2018). Osteohistology of the silesaurid *Sacisaurus agudoensis* from southern Brazil (Late Triassic) and implications for growth in early dinosaurs. *Anais da Academia Brasileira de Ciências*, 91. <https://doi.org/10.1590/0001-3765201920180643>.
- Wilson, J. A. (1999). A nomenclature for vertebral laminae in sauropods and other saurischian dinosaurs. *Journal of vertebrate Paleontology*, 19(4), 639–653.
- Wilson, J. A., D'Emic, M. D., Ikejiri, T., Moacdieh, E. M. & Whitlock, J. A. (2011). A nomenclature for vertebral fossae in sauropods and other saurischian dinosaurs. *PLoS ONE*, 6(2), e17114.
- Witmer, L. M. (1997). The evolution of the antorbital cavity of archosaurs: a study in soft-tissue reconstruction in the fossil record with an analysis of the function of pneumaticity. *Society of Vertebrate Paleontology, Memoir*, 3, 1–73. <https://doi.org/10.1080/02724634.1997.10011027>.
- Yates, A. M. (2003). A new species of the primitive dinosaur *Thecodontosaurus* (Saurischia: Sauropodomorpha) and its implications for the systematics of early dinosaurs. *Journal of Systematic Palaeontology*, 1(1), 1–4. <https://doi.org/10.1017/S1477201903001007>.
- Zerfass, H., Lavina, E. L., Schultz, C. L., Garcia, A. J. V., Faccini, U. F., & Chemale, J. F. (2003). Sequence stratigraphy of continental Triassic strata of Southernmost Brazil: a contribution to Southwestern Gondwana palaeogeography and palaeoclimate. *Sedimentary Geology*, 161(1-2), 85–105. [https://doi.org/10.1016/S0037-0738\(02\)00397-4](https://doi.org/10.1016/S0037-0738(02)00397-4).

Handling Editor: Daniela Schwartz.  
Phylogenetics Editor: Pedro Godoy.